

GENERATING SYNTHETIC CLINICAL DATA THAT CAPTURE CLASS IMBALANCED DISTRIBUTIONS WITH GENERATIVE ADVERSARIAL NETWORKS: EXAMPLE USING ANTIRETROVIRAL THERAPY FOR HIV

Nicholas I-Hsien Kuo¹,
 Federico Garcia², Anders Sönnernborg³, Maurizio Zazzi⁴, Michael Böhm⁵, Rolf Kaiser⁵,
 Mark Polizzotto⁶, Louisa Jorm¹, Sebastiano Barbieri¹

¹Centre for Big Data Research in Health, the University of New South Wales, Sydney, Australia

²Hospital Universitario San Cecilio, Granada, Spain

³Hospital Karolinska Institutet, Stockholm, Sweden

⁴Università degli Studi di Siena, Siena, Italy

⁵Uniklinik Köln, Universität zu Köln, Cologne, Germany

⁶Australian National University, Canberra, Australia

Corresponding author: Nicholas I-Hsien Kuo (n.kuo@unsw.edu.au)

ABSTRACT

Clinical data usually cannot be freely distributed due to their highly confidential nature and this hampers the development of machine learning in the healthcare domain. One way to mitigate this problem is by generating realistic synthetic datasets using generative adversarial networks (GANs). However, GANs are known to suffer from mode collapse thus creating outputs of low diversity. This lowers the quality of the synthetic healthcare data, and may cause it to omit patients of minority demographics or neglect less common clinical practices. In this paper, we extend the classic GAN setup with an additional variational autoencoder (VAE) and include an external memory to replay latent features observed from the real samples to the GAN generator. Using *antiretroviral therapy for human immunodeficiency virus* (ART for HIV) as a case study, we show that our extended setup overcomes mode collapse and generates a synthetic dataset that accurately describes severely imbalanced class distributions commonly found in real-world clinical variables. In addition, we demonstrate that our synthetic dataset is associated with a very low patient disclosure risk, and that it retains a high level of utility from the ground truth dataset to support the development of downstream machine learning algorithms.

Keywords: Machine Learning, Generative Adversarial Networks, HIV

ETHICS STATEMENT & REPRODUCIBILITY

This study was approved by the University of New South Wales' human research ethics committee (application HC210661). We based our synthetic HIV dataset on EuResist (Zazzi et al., 2012). For people in the EuResist integrated database, all data providers obtained informed consent for the execution of retrospective studies and inclusion in merged cohorts (Prosperi et al., 2010).

The EuResist Integrated DataBase (EIDB) can be accessed for scientific studies once a proposal for analysis has been approved by EuResist's Scientific Board (see: <http://engine.euresist.org/database/>). To facilitate future research, our code will be made available through https://github.com/Nic5472K/ScientificData2021_HealthGym. Our synthetic dataset is freely accessible through <https://healthgym.ai/>.

1 INTRODUCTION

Problem:	Synthetic clinical data can be used in place of highly confidential real data. However, their quality greatly impacts their utility to support the development of downstream models.
What is Already Known:	<i>Generative adversarial networks</i> (GANs) can generate realistic synthetic data but they are notorious for <i>mode collapse</i> – thus drastically decreasing the cohort diversity of generated data.
What this Paper Adds:	We propose a technique to mitigate mode collapse in generating clinical time series data. Of note, our synthetic data quality were particularly marked for data related to minority groups.

Advances in machine learning research for healthcare are hampered by an insufficient amount of openly available datasets. Clinical datasets are usually not readily accessible due to their confidential nature, and there is potential for patient harm if members of the cohort were to be successfully re-identified by an adversary (El Emam et al., 2020). One way to manage this risk is to generate realistic synthetic datasets that are sufficiently similar to their real counterparts (Goncalves et al., 2020). There is longstanding research in the field of synthetic data generation (Fienberg & Steele, 1998; Walonoski et al., 2018); and more recently, Li et al. (2021) and Kuo et al. (2022) showed promising results on generating mixed-type clinical time series data based on *generative adversarial networks* (GANs) (Goodfellow et al., 2014; Arjovsky et al., 2017; Gulrajani et al., 2017).

Unlike most generative models (Kingma & Welling, 2014; Sohl-Dickstein et al., 2015; Van Oord et al., 2016), GANs (Goodfellow et al., 2014) do not explicitly compute the data likelihood. Instead, they employ two sub-networks to solve a minimax game – a generator to synthesise data from a random latent prior, and a discriminator to distinguish real data from the synthetic data. When an optimal discriminator is employed and the divergence can be minimised between the real and the generated data distributions, the generator learns to model complex probability distributions.

While GANs have enjoyed a large amount of success in image generation (Yu et al., 2018; Karras et al., 2019) and their applications can also be found in both the natural language processing of text (Xu et al., 2018) and of speech (Pascual et al., 2017), they are not extensively studied in the medical domain. In fact, Goncalves et al. (2020) found that the promising MedGAN approach (Choi et al., 2017; Camino et al., 2018) performed unfavourably on the log-cluster metric (Woo et al., 2009) (see Section 4.3) indicating that their synthetic dataset was not sufficiently diversified¹.

A synthetic dataset that is highly representative of its real counterpart could be used to develop *reinforcement learning* (RL) (Sutton & Barto, 2018) algorithms. An RL agent could manage patient conditions from learning in an evolving clinical environment to construct a behaviour policy that optimises the duration, dosage, and type of treatment over time. However, learning from under-diversified synthetic datasets can lead to heavy biases in models and undermine fairness in patient care (Bhanot et al., 2021).

Generating realistic synthetic medical datasets is not a trivial task; and we attribute the difficulty to

- the highly sparse and strongly correlated nature of variables in real world clinical datasets (see Section 2.2), and
- the tendency of mode collapse to occur during GAN training (see Section 2.3).

We demonstrate that this algorithmic complication can be addressed by preconditioning the generator input. As illustrated in Figure 1, we extend the classic GAN setup with a *variational autoencoder* (VAE) (Kingma & Welling, 2014) and a buffer to externally store features encoded from the real data by the VAE encoder. Whereas the classic setup uses random values (Goodfellow et al., 2014), we sample and reparameterise features stored in the buffer as alternative generator inputs. For the rest of this paper, we will denote:

- $\mathcal{D}_{\text{real}}$ as the ground truth dataset;
- $\mathcal{D}_{\text{null}}$ as the null synthetic dataset generated using the classic GAN setup; and
- \mathcal{D}_{alt} as the alternative synthetic dataset generated using our modified GAN setup.

¹Refer to Table 7 and Figure 7 on page 16 of Goncalves et al. (2020). MedGAN failed to generate a synthetic dataset that faithfully represented multivariate categorical cancer data.

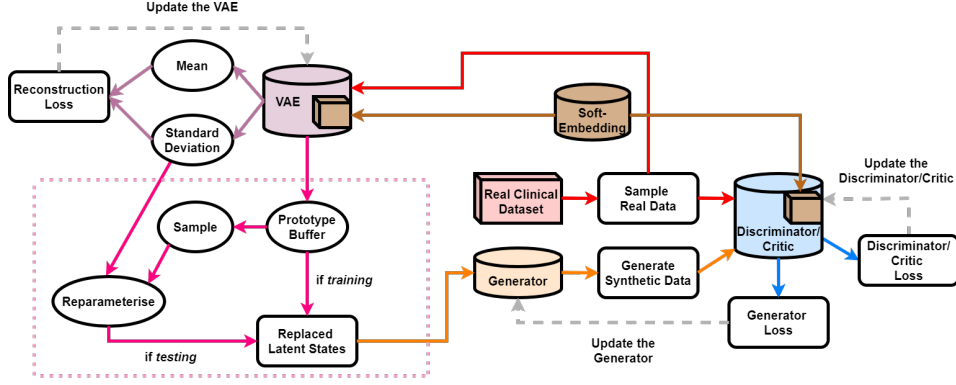


Figure 1: Extending GAN with a buffer replaying observed real data features.

In this paper, we use data related to *antiretroviral therapy for human immunodeficiency virus* (ART for HIV) as a case study. Optimising ART for HIV is non-trivial because a person with HIV usually requires changes in treatment regimens to avoid the development of drug-resistant viral strains (see Bennett et al. (2008) and Chapter 4 of a guideline published by the World Health Organisation (2016)). We observed that GAN generators with the classic random inputs synthesised *overly structured* outputs and cannot capture the diversity in the combination of medications in ART for HIV regimen (see Section 3.1). We found that not only did our extended GAN setup (see Section 3.2) increase the convergence rate, but it also captured severe class imbalanced combinations commonly found in real world clinical variables (see Section 5).

This significantly boosted the utility of the synthetic dataset (see Section 5.5). We found that RL agents trained on $\mathcal{D}_{\text{real}}$ and \mathcal{D}_{alt} would suggest similar clinical actions to manage health states in people with HIV. However, this was not achieved for an RL agent trained on $\mathcal{D}_{\text{null}}$. Our extended setup hence yielded a more reliable synthetic dataset which can be used to prototype RL algorithms in place of the highly confidential real data.

2 BACKGROUND

This section discusses the ground truth ART for HIV dataset, the practical problems in training GANs, and compares the recent work of Li et al. (2021) and Kuo et al. (2022) on successfully synthesising mixed type clinical datasets with GANs.

2.1 THE GROUND TRUTH ART FOR HIV DATASET

We selected a cohort of 8,916 people (with 332,800 records) from the EuResist database (Zazzi et al., 2012) using published inclusion/exclusion criteria (Kuo et al., 2022). There are 3 numeric, 5 binary, and 5 categorical variables, as listed in Table 1. The numeric variables – VL, CD4, and Rel CD4 – are indicative of the patient’s health status. The HIV treatment regimens are deconstructed as Base Drug Combo, Complimentary (Comp.) INI, Comp. NNRTI, Extra PI, and Extra pk-En. The medication classes are: nucleoside reverse transcriptase inhibitors (NRTIs), nucleotide reverse transcriptase inhibitors (NtRTIs), non-nucleotide reverse transcriptase inhibitors (NNRTIs), integrase inhibitor (INI), and protease inhibitors (PIs). The base drug combo mainly comprises NRTIs + NtRTIs; see Tang et al. (2012) for more details on the individual medications. There are 50 medication combinations in the real dataset spanning 21 medications.

The original EuResist database also contains a considerable proportion of missing data. Such information can be highly informative, indicating *e.g.*, the need for specific laboratory tests; and hence we include the variables with suffix (M) to indicate **if measurements are taken**. Measurements are taken (*i.e.*, entry with True) 24.27% for VL (M), 22.21% for CD4 (M), and 85.13% for Drug (M) in the real dataset $\mathcal{D}_{\text{real}}$.

Data in EuResist are collected irregularly hence we summarised it across calendar months (taking the last reported value for each variable of that month). There are often long gaps (over 6 months) in

Variable Name	Data Type	Unit	Valid Categorical Options
Viral Load (VL)	numeric	copies/mL	--
Absolute Count for CD4 (CD4)	numeric	cells/ μ L	--
Relative Count for CD4 (Rel CD4)	numeric	cells/ μ L	--
Gender	binary	--	Male; Female
Ethnicity (Ethnic)	categorical	--	Asian; African; Caucasian; Other
Base Drug Combination (Base Drug Combo)	categorical	--	FTC + TDF; 3TC + ABC; FTC + TAF; DRV + FTC + TDF; FTC + RTVB + TDF; Other
Complementary INI (Comp. INI)	categorical	--	DTG; RAL EVG; Not Applied
Complementary NNRTI (Comp. NNRTI)	categorical	--	NVP; EFV RPV; Not Applied
Extra PI	categorical	--	DRV; RTVB; LPV; RTV; ATV; Not Applied
Extra pk Enhancer (Extra pk-En)	binary	--	False; True
VL Measured (VL (M))	binary	--	False; True
CD4 (M)	binary	--	False; True
Drug Recorded (Drug (M))	binary	--	False; True

Table 1: The Variables of the ART in HIV Datasets

the original records; and hence we split such records into multiple shorter sub-records. We truncate the sub-records' lengths to the closest multiple of ten; as a result, the shortest record has 10 months of data and the longest has 100 months. Time series data including medication usage are valuable for developing algorithms to optimise illness management. A similar dataset was used in [Parbhoo et al. \(2017\)](#) to develop a hybrid approach of kernel-based regression and reinforcement learning for therapy selection. In the current paper, the generated synthetic data span 60 months of therapy for every patient, but the proposed setup can also be used to generate time-series of variable lengths.

2.2 THE HIGHLY SPARSE AND STRONGLY CORRELATED NATURE OF CLINICAL DATASETS

Option	Backbone	Comp. NNRTI	Comp. INI
A	TDF + FTC	EFV	N/A
B	TDF + FTC	NVP	N/A
C	TDF + FTC	N/A	DTG

Table 2: Three Examples of ART for HIV Treatments in Adolescents

As previously mentioned, treatment regimes for a person with HIV are changed to avoid developing drug-resistant viral strains (see [Bennett et al. \(2008\)](#) and Chapter 4 of [World Health Organisation \(2016\)](#)). A simple scenario with three common medication combinations² for adolescents is listed in Table 2 (the example medications include tenofovir (TDF), emtricitabine (FTC), efavirenz (EFV), nevirapine (NVP), and dolutegravir (DTG)). When we change the medications `OPTION A` \rightarrow `OPTION B`, the comp. NNRTI medication of `EFV` is replaced with the comp. NNRTI medication of `NVP`. When alternatively we change `OPTION A` \rightarrow `OPTION C`, `EFV` is replaced with the comp. INI medication of `DTG`.

For the examples shown in the table, sparseness arises (denoted as not applicable N/A) when an NNRTI medication is issued instead of an INI medication and vice versa. This also triggers *strong*

²See Table 4.3 on page 106 in [World Health Organisation \(2016\)](#).

(negative) correlations among different variables because the existence of an NNRTI medication leads to the non-existence of an INI medication. Learning to represent multivariate categorical dependencies is thus challenging and often requires researchers to make assumptions on the dependence structure of the data (Chow & Liu, 1968; Dunson & Xing, 2009).

2.3 MODE COLLAPSE WHILE TRAINING GANS

There are many known practical issues for training GANs (Kodali et al., 2017; Mescheder et al., 2018). In particular, *mode collapse* (Goodfellow, 2016) refers to the tendency of the GAN generator to collapse to a parametric setting where it always outputs the same point (or family of points); thus greatly reducing the diversity in GAN synthesised datasets.

We hypothesise that mode collapse is exacerbated by the highly sparse and strongly correlated nature of multivariate categorical clinical datasets. From Table 2, we see that since Options A, B, and C are all realistic, GAN can potentially learn to only output EFV whenever the comp. INI medication class is N/A. This is further complicated when the variable distributions are highly skewed (e.g., when EFV is prescribed more often than NVP), or when the distributions among different variables are imbalanced (e.g., when NNRTI medication is prescribed more often than INI medication).

Training GANs can be a difficult task. We aim to find a Nash equilibrium for the generator-discriminator pair (Goodfellow et al., 2014) which in practice is typically achieved using gradient descent techniques (e.g., SGD (Rumelhart et al., 1986) and Adam (Kingma & Ba, 2015)) rather than explicitly solving for the equilibrium strategy. Thus, training could fail to converge. Convergence in GANs can benefit from the careful selection of network modules (Radford et al., 2015), the change of learning objectives (Arjovsky et al., 2017; Gulrajani et al., 2017), and auxiliary experimental setups (Salimans et al., 2016; Sønderby et al., 2016). Nonetheless, the improvements for convergence in GAN training do not usually directly increase the quality of the generated data. As shown in Gulrajani et al. (2017) and in Liu et al. (2019), both studies found that synthetic images of higher qualities required the Lipschitz constraint to be enforced on the discriminator/critic network. However, Metz et al. (2016) also argued that by dropping variety (i.e., by allowing mode collapse), GAN could allocate more of its expressive power to fine-tune the few and already identified modes.

One approach to mitigate mode collapse used the learnt features within the GAN sub-networks to quantify diversity in the generated data. Salimans et al. (2016) used *minibatch discrimination* to project multiple copies of generated data to a high dimensional latent space and forwarded the differences in the latent features as an extra source of information to the discriminator. Li et al. (2017) adopted an encoder-decoder framework for their discriminator; and the encoder compartment of their discriminator encoded both the real and synthetic data. In addition to data generation, their architectural design allowed them to train their GAN to match various levels of abstractions (i.e., *moment matching*) in the encoded features of the real and synthetic data. In the same spirit, we explicitly store latent features of real data in an external buffer and replay them to the generator as a form of non-randomised prior at test time (see Figure 1).

Another line of study also showed that the generator outputs can benefit from employing discriminators with better designs or by having multiple discriminators (Srivastava et al., 2017; Mordido et al., 2020). Thanh-Tung & Tran (2020) found that mode collapse could be related to *catastrophic forgetting* (McCloskey & Cohen, 1989; Kuo et al., 2021) in the discriminator when the discriminator parameters escaped their previous local minimum. Mangalam & Garg (2021) found that this could be mitigated by sequentially introducing more discriminators.

2.4 ON CONCURRENTLY MODELLING MIX TYPED VARIABLES

While Gonçalves et al. (2020) showed that the traditional GAN approach encountered difficulties in generating multivariate categorical data, real life clinical data are even more complicated and usually consist of numeric, binary, and categorical variables. Two recent studies, Li et al. (2021) and Kuo et al. (2022), both reported the successful generation of mixed-type datasets using GANs.

On one hand, Li et al. proposed a generator with a pair of VAEs. While VAE-GANs (Larsen et al., 2016) were previously proposed to discover high-level disentangled representations in images, Li et al. used VAEs to map clinical variables of different types to a common feature representation

space – one VAE encoded the numeric variables, and the other encoded the non-numeric variables. [Li et al.](#) further included a matching loss to minimise the distance in the representation pairs.

On the other hand, [Kuo et al.](#)’s Health Gym GANs included a *soft-embedding* ([Mottini et al., 2018](#)) algorithm (see Figure 3). Their soft-embedding first created a small size lookup table for each binary and categorical variable; then they concatenated the lookup vectors with the numeric variables.

2.5 THE HEALTH GYM GAN

We based our work on [Kuo et al. \(2022\)](#)’s Health Gym GAN^{3,4}. Specifically, their generator G with weights η and critic C with weights κ were trained to optimise the losses,

$$L_C = \underbrace{\mathbb{E}[C(G(z))] - \mathbb{E}[C(x_{\text{real}})]}_{\text{Wasserstein value function}} + \underbrace{\lambda_{\text{GP}} \mathbb{E}[(\|\nabla_{\tilde{x}_{\text{syn}}} C(\tilde{x}_{\text{syn}})\|_2 - 1)^2]}_{\text{Gradient penalty loss}} \quad \text{and} \quad (1)$$

$$L_G = -\mathbb{E}[C(G(z))] + \underbrace{\lambda_{\text{corr}} \sum_{i=1}^n \sum_{j=1}^{i-1} \text{abs}\left(r_{\text{syn}}^{(i,j)} - r_{\text{real}}^{(i,j)}\right)}_{\text{Alignment loss}}, \quad (2)$$

following the *Wasserstein GAN with gradient penalty* (WGAN-GP) setup ([Gulrajani et al., 2017](#)). In Equation (1), $G(z) = x_{\text{syn}}$ denoted the synthetic data generated from the generator with random input z ; x_{real} is the real data sampled from the database; \tilde{x}_{syn} is interpolated between $G(z)$ and x_{real} ; and λ_{GP} is a constant that manages the strength of the gradient penalty loss. Furthermore, [Kuo et al.](#) introduced an *alignment loss* in Equation (2) to ensure that the correlations do not diverge among variables during training. The alignment loss is computed as the sum of the absolute differences in the *Pearson’s r correlation* ([Mukaka, 2012](#)) for all pairs of distinct variables $i \neq j$ between the synthetic data $r_{\text{syn}}^{(i,j)}$ and their real counterparts $r_{\text{real}}^{(i,j)}$. A constant λ_{corr} is employed to manage the strength of the alignment loss.

During our experiments, we found that [Kuo et al.](#)’s WGAN-GP setup was able to converge without the alignment loss but could not synthesise meaningful data. Hence similar to the observation made in [Metz et al. \(2016\)](#), the convergence in GAN did not imply the acquisition of the ability to generate high quality output (see Section 2.3). In contrast, the approach that we developed in this paper is capable of converging quickly and produces highly realistic data without the auxiliary objective.

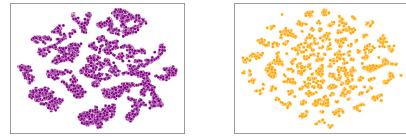
3 MATERIALS AND METHODS

We introduce an additional VAE and an extra buffer to extend [Kuo et al. \(2022\)](#)’s WGAN-GP setup.

3.1 DATA, VISUALISED FROM THE PERSPECTIVE OF THE CRITIC

To illustrate the mode collapse problem, we first trained [Kuo et al. \(2022\)](#)’s WGAN-GP until convergence. Then, we created batches of synthetic data $G(z) = x_{\text{syn}}$ using random inputs z ; and passed both x_{syn} and the real dataset x_{real} to their critic C . We extracted the features encoded in the critic’s soft-embedding (a form of intermediate features, see Figure 3) as f_{syn} and f_{real} respectively; and then concatenated f_{syn} and f_{real} , and used t-SNE ([Van der Maaten & Hinton, 2008](#)) to project the features in \mathbb{R}^2 and plotted them in Figure 2.

The features f_{syn} shown in subplot 2(a) resembles that of a collection of clusters, while f_{real} in subplot 2(b) are much more evenly distributed in space. The overly structured f_{syn} indicated that the



(a) The f_{syn} features. (b) The f_{real} features.

Figure 2: t-SNE visualisations of the soft-embedding features.

³See their codes in https://github.com/Nic5472K/ScientificData2021_HealthGym.

⁴The critic in the WGAN setting ([Arjovsky et al., 2017](#)) is equivalent to the discriminator of the traditional GAN setup. It is called a critic since it’s not trained to classify outputs but to score their realismness instead.

generator experienced mode collapse and thus created very similar groupings of synthetic patient records and are less diversified than the real patient records.

3.2 FEATURE REPLAY AS A FORM OF GENERATOR INPUT

Larsen et al. (2016)’s VAE-GAN showed that smooth image interpolation could be achieved via adding attribute vectors to the learned VAE latent features. Inspired by their finding, we also extended Kuo et al. (2022)’s WGAN-GP setup with a VAE to generate variations of synthetic patient records. However, instead of sampling new latent features from the VAE learnt parameterised distributions, we externally stored and replayed the features of real data in a buffer (see Figure 1).

Tied Soft-Embedding

As shown in Figure 3, Kuo et al.’s critic includes a *soft-embedding* mechanism followed by a feature extraction block. Soft-embedding acts like word embedding (Mikolov et al., 2013) and helps the critic to concurrently learn features for a mixed-type dataset.

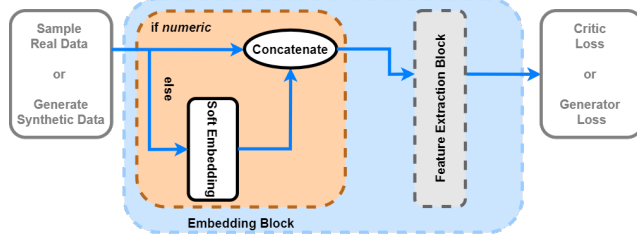


Figure 3: The critic.

A lookup vector is created for each available option in the binary (e.g., male in gender) and categorical (e.g., DTG in comp. INI, see Table 2) variables. Unlike the classic word embedding where all tokens shared the same embedding dimension (e.g., 400 dimensions per embedding for every word), soft-embedding allows each clinical variable to have a distinct dimensionality (e.g., 2 dimensions per class for each binary variable and 4 dimensions per class for each categorical variable). The vector representations are then concatenated with the values of the numeric variables before being further processed by the feature extraction block.

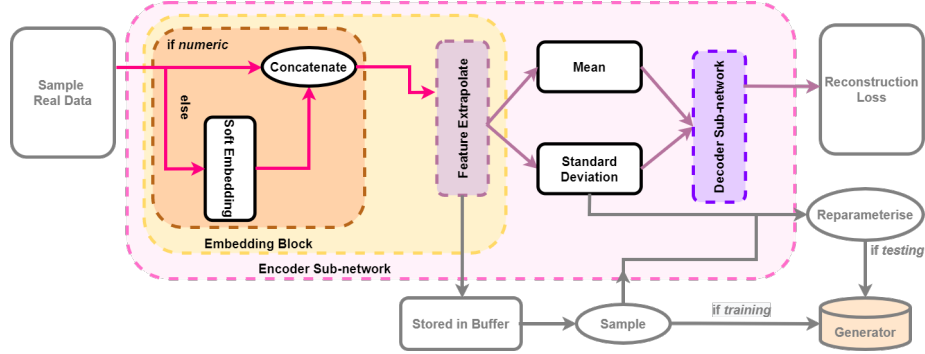


Figure 4: The VAE, with soft-embedding tied to the critic.

In our extended setup, we introduce the VAE in Figure 4 with soft-embedding in its encoder. We tie the soft-embedding weights in the VAE encoder to those in the critic and hence it also observes real data. Then, we store a transformed representation f_{real} from the real data (similar to that in Figure 2(b)) in a fixed size external buffer. We replay f_{real} as a form of non-random inputs to the generator.

Our Extra VAE

A conventional VAE V , with encoder weights ϕ and decoder weights θ , is trained by optimising

$$L_V = \underbrace{-\lambda_{\text{KL}} \text{KL}(q_\phi(\xi|x_{\text{real}})||p_\theta(\xi))}_{\text{KL divergence}} + \underbrace{\mathbb{E}_{q_\phi(\xi|x_{\text{real}})} \log(p_\theta(x_{\text{real}}|\xi))}_{\text{Log-likelihood reconstruction loss}}. \quad (3)$$

L_V consists of the KL divergence to approximate the posterior q from the prior p , and a log-likelihood term to reconstruct \hat{x}_V for the real data x_{real} from the latent variable ξ ; in addition, λ_{KL} is a constant term to manage the strength of the KL divergence.

We select a Gaussian distribution as the prior p . As shown in Figure 4, our VAE encoder shares the critic’s soft-embedding to encode the real data as features γ_{real} and the learned standard deviations

Algorithm 1 Training an Extended WGAN-GP with a VAE and a buffer.

Initialises network parameters: VAE's ϕ and θ , as well as generator's η , and critic's κ
Initialises an external buffer: $\mathcal{B} \leftarrow \emptyset$

1: **repeat**
 # Training the VAE $V_{\phi, \theta}$
2: Sample real data $x_{\text{real}} \leftarrow \mathcal{D}_{\text{real}}$
3: Apply the VAE $\xi, \gamma_{\text{real}}, \sigma_V, \hat{x}_V \leftarrow V_{\phi, \theta}(x_{\text{real}})$
4: Compute the VAE loss see Equation (3)
5: Update the VAE parameters $\phi, \theta \stackrel{+}{\leftarrow} -\nabla_{\phi, \theta} L_V$
6: Release space from the buffer if full $\mathcal{B} \stackrel{\text{release}}{\leftarrow} \text{cardinality of } \gamma_{\text{real}}$
7: Append the buffer $\mathcal{B} \leftarrow \mathcal{B} \oplus \gamma_{\text{real}}$

 # Training the critic C_{κ}
8: **for** $t = 1, \dots, n_{\text{critic}}$ **do**
9: Sample real data $x_{\text{real}} \sim \mathcal{D}_{\text{real}}$, sample stored features $\gamma_{\text{real}} \sim \mathcal{B}$,
 and sample random numbers for interpolation $\epsilon \sim U[0, 1]$
10: Generate synthetic data $x_{\text{syn}} \leftarrow G_{\eta}(\gamma_{\text{real}})$
11: Syn-Real data interpolation $\tilde{x}_{\text{syn}} \leftarrow \epsilon x_{\text{real}} + (1 - \epsilon)x_{\text{syn}}$
12: Compute the critic loss see Equation (1)
13: Update the critic parameters $\kappa \stackrel{+}{\leftarrow} -\nabla_{\kappa} L_C$
14: **end for**

 # Training the generator G_{η}
15: Sample stored features $\gamma_{\text{real}} \sim \mathcal{B}$
16: Generate synthetic data $x_{\text{syn}} \leftarrow G_{\eta}(\gamma_{\text{real}})$
17: Compute the generator loss see Equation (2)
18: Update the generator parameters $\eta \stackrel{+}{\leftarrow} -\nabla_{\eta} L_G$
19: **until converge**

(std-s) σ_V . Then, we sample latent variables $\xi \leftarrow \gamma_{\text{real}} + \rho$ where $\rho \sim N(0, \sigma_V)$ for the VAE decoder to reconstruct \hat{x}_V .

During training, the GAN generator receives different inputs to the VAE decoder. While the VAE decoder receives latent variables ξ , the GAN generator receives the unmodified features γ_{real} (*i.e.*, $z \leftarrow \gamma_{\text{real}}$). In addition, we employ an external buffer \mathcal{B} to collect γ_{real} .

At test time, we discard the VAE and sample stored features (with replacement) from the buffer for the GAN generator $\overline{\gamma_{\text{real}}} \sim \mathcal{B}$. The goal of the feature replay mechanic is to avoid mode collapse by establishing a dependency between the generator output and the highly diversified ground truth latent features of the real data γ_{real} . However, since we aim to create new synthetic patient records, the generator input are reparameterised as $z \leftarrow \overline{\gamma_{\text{real}}} + \rho^*$ where $\rho^* \sim N(0, \sigma_V)$.

Our Feature Replay Mechanic & Algorithmic Overview

An overview for training our extended WGAN-GP is presented in Algorithm 1. For each iteration, we train the components in the order of: the VAE with Equation (3), the critic with Equation (1) for a pre-defined inner-loop n_{critic} (Gulrajani et al., 2017), and the generator with Equation (2). Our external buffer \mathcal{B} has a fixed size; when no vacancy is left in \mathcal{B} (see Line 6), we randomly release space in \mathcal{B} to append the new encoded features γ_{real} (see Line 7). There are alternative ways to update the buffer, such as *herding* (Welling, 2009) for constructing an exemplar set (Rebuffi et al., 2017); but the search for an optimal buffer update mechanism is out of the scope of this paper.

3.3 ON VAES: TO REPLAY OR TO SAMPLE

While both our approach and Larsen et al. (2016)'s VAE-GAN employ a VAE in conjunction with a GAN, there are three important distinctions. First, Larsen et al. combine the VAE decoder with the GAN generator while our setup keeps the sub-networks distinct: our VAE decoder has weights θ and the GAN generator has weights η . Second, Larsen et al. implement a different reconstruction loss for

the VAE. Instead of using the exact differences between the original input x_{real} and the reconstructed outcome \hat{x}_V , they take the average of all differences in the features of the intermediate layers in the decoder⁵. This is similar to Li et al. (2017)’s moment matching practice discussed in Section 2.3.

The third and most important difference lies in the relationship between the VAE encoder output and the generator input. In their work, the inputs of Larsen et al.’s generator (merged with the decoder) are sampled from the learned distribution of the VAE encoders. In our study, we store all features γ_{real} encoded from the real data and replay them to the generator (see Lines 9 and 15 in Algorithm 1). Replaying γ_{real} provides exact combinations of information in the latent structure of x_{real} to the generator and helps GAN to capture real data in the sparse feature space (see Section 2.2).

4 EXPERIMENTAL SETUPS

This section includes the hyper-parameter settings, the baseline models, and the metrics used in our experiments.

4.1 HYPER-PARAMETERS

Module Selection

Our extended WGAN-GP setup inherited most of the hyper-parameters from Kuo et al. (2022)⁶ including the identical designs for the generator G and critic C . The generator had 1 bidirectional *long short-term memory* (bi-LSTM) (Hochreiter & Schmidhuber, 1997; Graves et al., 2005) followed by 3 linear layers. The critic used 2 and 4 as the hidden dimensions in soft-embedding for the binary and categorical variables respectively; then in the feature extraction block, it included 2 linear layers followed by 1 bi-LSTM and 1 additional linear layer. The input and hidden dimensions of G were 128. The hidden dimension for C was also 128; and the input dimension was 29 (from concatenating the soft-embeddings of 3 numeric, 5 binary, and 4 categorical variables $3 + 5 \times 2 + 4 \times 4 = 29$).

The encoder in the VAE V shared the soft-embedding in the critic. The encoder then employed 4 linear layers with *residual connections* (He et al., 2016) between each layer for feature extrapolation. The decoder of V had 1 linear layer. The hidden dimension of V was 128 hence $\gamma_{\text{real}}, \sigma_V \in \mathbb{R}^{128}$ (matching the input dimension of the generator). Since the VAE shared the soft-embedding of C , V ’s input dimension was 29.

The latent features encoded from real data were stored in a fixed size buffer (see Lines 6 and 7 in Algorithm 1). We defaulted the buffer size to 10,000 samples, storing roughly 3% of all real data. However, we also tested when less memory was allocated.

Optimisation Setup

The sub-networks G , C , and V were all trained using Adam (Kingma & Ba, 2015) with learning rate 0.001 for 200 epochs with batch size 256. We set the regularisation coefficients in GANs as $\lambda_{\text{GP}} = 10$ and $\lambda_{\text{corr}} = 10$ (see Equations (1) and (2)); and $\lambda_{\text{KL}} = 1$ (see Equation (3)) for the VAE. In addition, we updated C for $n_{\text{critic}} = 5$ steps (see Line 8 of Algorithm 1) for every update in G .

As we previously discussed in Section 2.5, the alignment loss regularised with λ_{corr} was introduced in Kuo et al. (2022) to stabilise GAN training. In our extended WGAN-GP training we included the alignment loss; but we also tested performance without the auxiliary loss. Furthermore, the medication records of ART for HIV have non-uniform lengths (see Section 2.1). The shortest record was 10 units long and the longest record was 100 units long; hence we employed *curriculum learning* (Bengio et al., 2009) to sequentially expose our models to longer records.

4.2 BASELINE MODELS

We refer to Kuo et al. (2022)’s setup as **WGAN-GP** and ours as **WGAN-GP+VAE+Buffer**.

Alternative Architectural Designs

While the original **WGAN-GP** reported competitive results, it could potentially benefit from being

⁵See Equation 7 on page 2 of Larsen et al. (2016).

⁶See Fig. 1 in page 14 of Kuo et al. (2022); and their repository in footnote 3.

equipped with alternative modules that were developed more recently. Both the critic and the generator of **WGAN-GP** employed LSTMs (Hochreiter & Schmidhuber (1997), see Section 4.1). We tested various ways to substitute their LSTMs with – Transformer (Vaswani et al., 2017), BERT-like encoder-only Transformer (Kenton & Toutanova, 2019), and GPT-like decoder-only Transformer (Radford et al., 2018). We found that the best combination resulted from replacing the bi-LSTM in the generator with encoder-only Transformers (EOTs). We implemented two versions of GAN with EOT:

WGAN-GP+G_EOT with EOT naïvely implemented; and
WGAN-GP+G_EOT+VAE+Buffer when EOT was implemented along with our extended setup.

Our EOT modules processed input data sequentially with 3 sets of multi-head scaled dot-product attention. Following the setting in Section 4.1, the input and hidden dimensions were 128 and we employed 8 heads. Importantly, attention mechanism was applied to the temporal dimension⁷. In addition, there were 100 lookup vectors in the EOT positional embedding; this was because the longest ART for HIV record was 100 units long.

We tested Larsen et al. (2016)’s VAE-GAN against our WGAN-GP+G_EOT; see Section 3.3 for an in-depth comparison of the two models. A VAE encoder was added on top of Kuo et al.’s original design (with gradient penalty included) and we referred to it as VAE-WGAN-GP.

Previous Methods that Aim to Mitigate Mode Collapse

We further extended **WGAN-GP** with 3 techniques that were initially proposed to mitigate the mode collapse of GANs for image generation (see Section 2.3): WGAN-GP+MBD with minibatch discrimination (MBD) (Salimans et al., 2016), WGAN-GP+MM with moment matching (MM) (Li et al., 2017), and WGAN-GP+MC with multiple critics (MC) (Mangalam & Garg, 2021). Specifically, WGAN-GP+MBD was implemented with projection matrices of size $\mathbb{R}^{3 \times 5}$ after the embedding block and before the feature extraction block of the critic; WGAN-GP+MM matched the features encoded by the critic embedding block; and we introduced a new critic every 50 epochs for WGAN-GP+MC.

4.3 METRICS

There are 5 desiderata: a) that our technique mitigates mode collapse in the GAN generator; b) that all generated variables are individually realistic; c) that all variables are also collectively realistic over time; d) that our synthetic datasets are highly secure and do not disclose patient identity; and last e) that our dataset has high utility and can substitute a real dataset for downstream model building.

4.3.1 MITIGATING MODE COLLAPSE

Following Goncalves et al. (2020), we employ the *log-cluster* metric U (Woo et al., 2009)

$$U = \log \left(\frac{1}{\Gamma} \sum_{k=1}^{\Gamma} \left[\frac{n_{k_{\text{real}}}}{n_k} - \frac{n_{k_{\text{real}}}}{n_{k_{\text{real}}} + n_{k_{\text{syn}}}} \right]^2 \right) \quad (4)$$

to estimate the difference in latent structures between the real and the synthetic datasets. First, we sample records from both the real and synthetic datasets. Then, we merge the sub-datasets and perform a cluster analysis via k-means with $\Gamma = 20$ clusters. We denote n_k as the total amount of records in cluster k ; and $n_{k_{\text{real}}}$ and $n_{k_{\text{syn}}}$ are the respective number of real and synthetic records in the cluster. U thus measures the logged average cluster-wise divergence. We repeat this process for 20 times for each synthetic dataset; and each time we sample 100,000 real and synthetic records. The lower the U score, the more realistic the synthetic datasets.

In addition to the log-cluster metric, we also include the *category coverage* (CAT) metric

$$\text{CAT} = \frac{1}{\mathcal{U}} \sum_{u=1}^{\mathcal{U}} \frac{\|\mathcal{D}_{\text{syn}}^{(u)}\|}{\|\mathcal{D}_{\text{real}}^{(u)}\|} \quad (5)$$

proposed in Goncalves et al. (2020). For all binary and categorical variables $u = 1, \dots, \mathcal{U}$, we find the number of unique levels $\|\cdot\|$ of the u -th variable in the synthetic dataset \mathcal{D}_{syn} and its real

⁷Attention mechanism was not applied to the feature dimension (*i.e.*, the clinical variables in Table 1). This was because in their paper, Kuo et al. (2022) found that their simpler LSTM-based GAN was already capable of capturing correlations between clinical variables.

counterpart $\mathcal{D}_{\text{real}}$. The higher the CAT score ($\text{CAT} \in [0, 1]$), the more complete the non-numeric classes in the synthetic datasets and the less likelihood of mode collapse in the GAN generators.

While convergence does not directly guarantee the generation of high quality synthetic datasets (see Section 2.3); GANs that do not converge are unlikely to generate good results. Our convergence metric is based on the correlation loss $L_{\text{corr}} = \sum_{i=1}^n \sum_{j=1}^{i-1} \text{abs} \left(r_{\text{syn}}^{(i,j)} - r_{\text{real}}^{(i,j)} \right)$ of Equation (2); and we record this score for every iteration during the GAN training phase. This allows us to know whether the models are learning; and whether the relations among the clinical variables are learned. The lower the L_{corr} score, the better represented the correlations among the synthetic data variables.

4.3.2 REALISTICNESS OF THE INDIVIDUAL VARIABLES

The individual realisticness of each variable can be checked with 2 types of plots. For the numeric variables, we superimpose the synthetic distribution over their real counterparts using *kernel density estimations* (KDEs) (Davis et al., 2011). As for the binary and categorical variables, we show the percentage share of each option using side-by-side barplots.

Following Kuo et al. (2022), we perform 4 statistical tests on the synthetic datasets organised as shown in Figure 5. We start with the two-sample Kolmogorov-Smirnov (KS) test (Hodges, 1958) to check whether the synthetic variables capture details of the distributions of their real counterparts. If a synthetic variable passes the KS test, the synthetic data is realistic and is considered to have been drawn from the real database. If a synthetic variable fails the KS test, we also aim to understand why it is considered non-realistic.

The two independent sample Student’s t-test (Yuen, 1974) and F-test (numeric: Snedecor’s F-test (Snedecor & Cochran, 1989); otherwise: the analysis of variance F-test) are useful techniques to understand why a synthetic variable would be considered unrealistic. The former checks the alignment between the synthetic and real mean; while the latter verify the alignment with the synthetic and real variance.

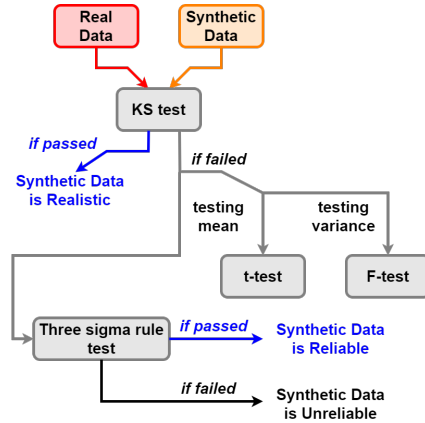


Figure 5: Statistical tests.

While the t-test and F-test could help us identify the shortcomings of a synthetic variable, they cannot assess the reliability of a synthetic variable if it fails the KS test. To this end, we employ the three sigma rule test (Pukelsheim, 1994) (defaulted with 2 std-s) to check if the values in the synthetic variable fall in a probable range of real variable values.

4.3.3 FIDELITY IN VARIABLE CORRELATIONS

We compute Kendall’s τ rank correlation (Kendall, 1945) to compare the relationships of the variables in the mixed-type datasets⁸. The correlation is computed in 2 different ways. First, we compute the *static* correlations among all data points under the classic setup. Second, we follow the practice in Kuo et al. (2022) and estimate the average *dynamic* correlations.

The dynamic correlation is computed in two parts. First, we take all records of a patient p and linearly deconstruct each variable i into a trend with cycle

$$X_p^{(i)} = \text{Trend}(X_p^{(i)}) + \text{Cycle}(X_p^{(i)}). \quad (6)$$

Trends describe macroscopic behaviours in the time series data (*i.e.*, increasing or decreasing over time); and cycles helps us understand information on the microscopic level (*e.g.*, periodic behaviours). After detrending the variables, we compute the correlations in both the trends and cycles; and then we average the values across all patients.

⁸Unlike Pearson’s correlation (Mukaka, 2012), Kendall’s correlation can be applied to both numeric and non-numeric variables; and also between a numeric and non-numeric pair of variables.

4.3.4 PATIENT DISCLOSURE RISK

We conduct two tests to check whether our synthetic datasets are highly secure for public access. First, we verify that the minimum Euclidean distance between all synthetic records and real records is greater than zero thus no real record is leaked into the synthetic datasets. Then, we use [El Emam et al. \(2020\)](#)’s *sample-to-population attack* to check if an attacker can learn new information by matching an individual from the synthetic datasets to the real datasets.

[El Emam et al.](#) estimated the patient exposure risk via *quasi-identifiers* – special variables that may reveal the identity of a person. The quasi-identifiers in the ART for HIV dataset are *Gender* and *Ethnicity*. Equivalent classes are made from combinations of quasi-identifiers (e.g., *Male + Asian* and *Female + African*). Then, for every synthetic patients s , we compute

$$\frac{1}{S} \sum_{s=1}^S \left(\frac{1}{F_s} \times I_s \right) \quad (7)$$

to estimate the chance of matching a random individual in the synthetic dataset to an individual in the real dataset. S is the total records in the synthetic dataset, $I_s \in \{0, 1\}$ equals to one if the equivalent class of synthetic s is present in both datasets (e.g., *Male + Asian* appears in both the real and synthetic datasets), and F_s is the cardinality of the equivalent class in the real dataset (i.e., the target dataset). The [European Medicines Agency \(2014\)](#) and [Health Canada \(2014\)](#) have both suggested that this risk should be no more than 9% to balance security and synthetic data utility⁹.

4.3.5 UTILITY VERIFICATION

We compare RL agents trained on both the real and synthetic datasets. Then, we claim that a synthetic dataset has a high level of utility if the two trained RL agents suggest similar actions to treat patients; implying that the synthetic dataset can be used in place of the real dataset to support the development of downstream machine learning applications.

We define a set of observational variables \mathcal{D}_O and a set of action variables \mathcal{D}_A from Table 1 to train our RL agents. In our experiments, \mathcal{D}_O comprises the three numeric variables – VL, CD4, and Rel CD4 – at the current time step t ; and all of the medications used in the previous time step $t - 1$ (five variables, as described in Section 2.1). The three numeric variables inform us of a patient’s health state, and we factor information of previous regimens to consider the likelihood of formation of drug-resistant viral strains (see Section 2.2).

We follow the work of [Liu et al. \(2021\)](#) to define clinical states from the observation variables \mathcal{D}_O . We first apply cross decomposition ([Wegelin, 2000](#)) to reduce the dimensionality of \mathcal{D}_O to 5. Then, we perform K-Means clustering ([Vassilvitskii & Arthur, 2006](#)) with 100 clusters to label each data point in \mathcal{D}_O using their associated clusters.

While the observation variables always consist of the same set of variables, we compare various setups for defining the action variables \mathcal{D}_A . In one of our setups, we reserve Base Drug Combo and Comp. NNRTI to span the action space A , resulting in 24 ($= 6 \times 4$) unique actions. Refer to Section 5.5 for all of our setups.

Our RL method of choice is batch-constrained Q-learning ([Fujimoto et al., 2019](#)). In each setup, we update the policy for 100 iterations with step size 0.01. Several alternative offline RL methods ([Levine et al., 2020](#)) have recently been developed; but we employ RL in this paper to verify synthetic dataset utility, and hence a large scale comparison over different RL techniques is out of the scope of this study.

We update the RL policy using the reward function adapted from [Parbhoo et al. \(2017\)](#). The reward function is given as

$$\text{reward}_t = \begin{cases} -0.7 \log \text{VL}_t + 0.6 \log \text{CD4}_t, & \text{if VL}_t \text{ is above detection limits, and} \\ 5 + 0.6 \log \text{VL}_t & \text{if VL}_t \text{ is below detection limits.} \end{cases} \quad (8)$$

Note, we use cells/ μL as the unit for CD4_t count in Table 1, while [Parbhoo et al.](#) use cells/mL as their unit for the reward computation in Equation (8).

⁹For the [European Medicines Agency \(2014\)](#), refer to Sec. 5.4 clause 4 on page 47. For [Health Canada \(2014\)](#), refer to Sec. 6.2 under the Risk Threshold subsection.

5 RESULTS

This section evaluates the five desiderata outlined in Section 4.3.

5.1 MODE COLLAPSE AND TRAINING STABILITY

Table 3: Metric comparisons. \downarrow : the lower the better; \uparrow : the higher the better.

	Logged correlation (L_{corr}) (\downarrow)	Log-cluster (U) (\downarrow)	Category coverage (CAT) (\uparrow)
WGAN-GP (Kuo et al., 2022)	-7.91	-2.11 ± 0.02	0.98
WGAN-GP+VAE+Buffer (Ours)	-8.09	-2.65 ± 0.05	1.00
WGAN-GP+G_EOT+VAE+Buffer (Ours)	-7.97	-3.00 ± 0.02	1.00
VAE-WGAN-GP (Larsen et al., 2016)	-7.86	-2.24 ± 0.04	0.93
WGAN-GP+MBD (Salimans et al., 2016)	-7.32	-1.79 ± 0.04	0.90
WGAN-GP+MM (Li et al., 2017)	-7.49	-2.31 ± 0.03	0.95
WGAN-GP+MC (Mangalam & Garg, 2021)	-7.93	-2.27 ± 0.03	0.93

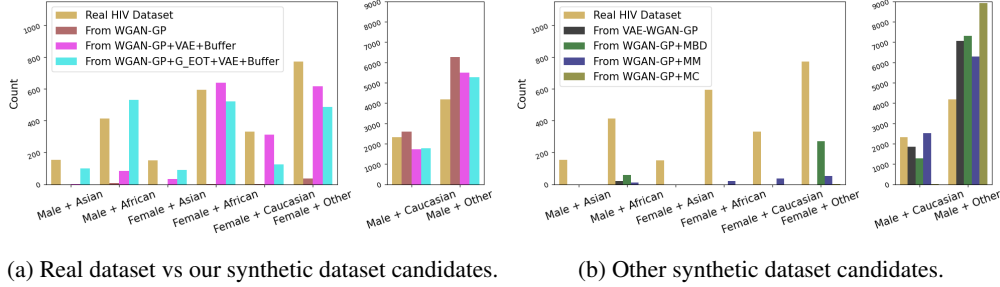


Figure 6: Inspecting mode collapse on the gender-ethnicity pair.

5.1.1 ON MITIGATING MODE COLLAPSE

After training seven variants of GANs for generating ART for HIV data, we compared their synthetic datasets using the metrics discussed in Section 4.3.1 and aggregated the results in Table 3. We found that our extra VAE with external buffer performed more favourably in mitigating mode collapse. Specifically, the lower log-cluster scores indicate that our synthetic datasets \mathcal{D}_{alt} are better at mirroring the latent structure in the ground truth $\mathcal{D}_{\text{real}}$ (refer to the denotations in Section 1). In addition, both of our \mathcal{D}_{alt} score 1.00 in category coverage, thus they cover all categories that can be found in $\mathcal{D}_{\text{real}}$. While these quantitative analyses provided an easy way to quickly compare multiple GAN designs, these metrics remain purely relative and do not carry any physical meaning. We hence conducted a qualitative study to investigate the impact of mode collapse.

We plotted the frequency of all *gender-ethnicity* pairs in Figure 6. Subplot 6(a) showed that the synthetic dataset $\mathcal{D}_{\text{null}}$ generated using Kuo et al. (2022)’s WGAN-GP indicated mode collapse and created synthetic patients of mostly *Male+Caucasian* and *Male+Other*. In contrast, our synthetic datasets \mathcal{D}_{alt} generated from WGAN-GP+VAE+Buffer and WGAN-GP+G_EOT+VAE+Buffer captured both genders for all ethnicity.

We also found that previous methods that were proposed to mitigate mode collapse in computer vision were not very effective for clinical time-series. In subplot 6(b), the synthetic datasets generated using MBD (Salimans et al., 2016), MM (Li et al., 2017), and MC (Mangalam & Garg, 2021) all behaved similarly to (or worse than) Kuo et al.’s baseline. These techniques were likely ineffective due to the unique challenges in real life clinical datasets previously mentioned in Section 2.2.

Figure 6 also showed that mode collapse in GANs would decrease cohort diversity through omitting patients of minority background (e.g., Asian males and African females). This meant that if we were to ignore mode collapse and use the synthetic dataset $\mathcal{D}_{\text{null}}$ to develop downstream RL agents, we

would not be able to suggest optimal treatments for under-represented patients. See more results in Section 5.5 regarding utility verification.

5.1.2 ABLATION STUDY ON REPLAY DIVERSITY

Overall, our **WGAN-GP+G_EOT+VAE+Buffer** performed most favourably across our metrics. However, the success of this setup came with the extra memory cost from the use of the external buffer. In order to test the robustness of our novel setup, we reduced the buffer from a large size of 10,000 samples to a small size of 500 samples; and to a tiny size of 25 samples. The large buffer stored 3.00% of HIV records, and the small and tiny buffers stored 0.15% and 0.008% of records, respectively¹⁰.

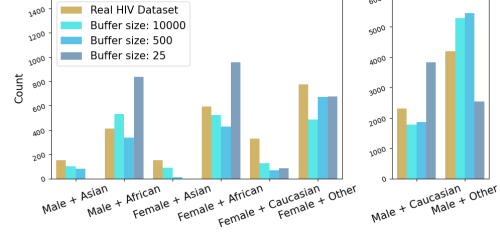


Figure 7: Inspecting buffers of different sizes.

The test results in Figure 7 show that the larger the buffer size the higher the quality of the synthetic dataset. Both the large and small buffers helped our setup to generate patients of all demographics, but the tiny buffer had difficulties in creating Asian patient records. Note, the tiny buffer size still produced a synthetic dataset of higher quality than [Kuo et al. \(2022\)](#)’s **WGAN-GP** (see Figure 6(a)).

5.1.3 TRAINING STABILITY

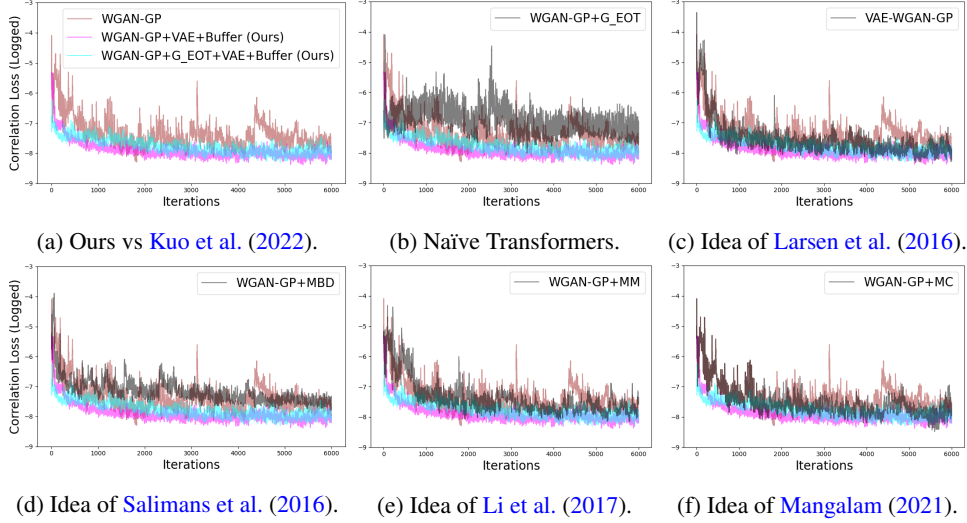


Figure 8: The logged correlation loss of the first 200 epochs.

As discussed in Section 2.3, the instability experienced by GANs during training is highly entwined with mode collapse. In Figure 8, we illustrated the correlation loss L_{corr} during the training phase of different GAN variants; and we observed in subplot 8(a) that the additional VAE and extra buffer in our **WGAN-GP+VAE+Buffer** and **WGAN-GP+G_EOT+VAE+Buffer** were beneficial for achieving lower loss in less time. While the other baseline models also converged, their optimisation were not as smooth and Table 3 showed that they scored worse in the final L_{corr} metric.

Some interesting observations were made when we replaced the LSTMs with Transformers in the GAN generator. Subplot 8(b) demonstrates that a naïve replacement would lead to worse results; and subplot 8(a) shows that *Transformers could perform more favourably than LSTMs when implemented along with our extended replay mechanism*. This is likely because Transformer’s attention mechanism ([Bahdanau et al., 2015](#)) acted as a form of weighted aggregation. Under the classic GAN setup, randomly sampled vectors were forwarded to the Transformer in the GAN generator

¹⁰See Section 2.1, the real HIV dataset contains 332, 800 records in total.

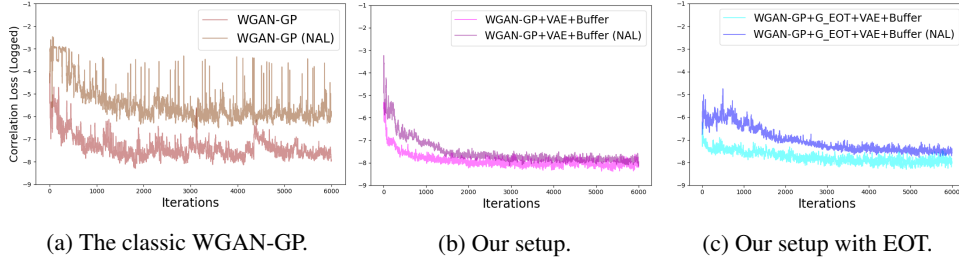


Figure 9: Training with and with no alignment loss (NAL).

as inputs, and attention weights assigned to such random vectors were not meaningful. In contrast, our replay algorithm supplied the Transformer in the GAN generator with information on the latent structure of the real data; Transformer’s attention mechanism was hence able to extract meaningful information to enhance the quality of synthetic data.

We further tested the training stability of GANs with no alignment loss (NAL) (see Equation (2)). As shown in Figure 9, the alignment loss was essential for updating Kuo et al. (2022)’s WGAN-GP. Without this auxiliary learning objective, WGAN-GP converged to a larger minimum loss indicating that its generated data was less realistic. In contrast, our extended GAN optimised successfully under the NAL scenario; no explicit assumptions on the data structure was therefore required for generating our synthetic data. Nonetheless, training was faster with the alignment loss employed.

5.2 REALISTICNESS OF THE INDIVIDUAL VARIABLES

Figure 10 presents the KDE plots and side-by-side barplots for the individual variable comparisons. The real variables from $\mathcal{D}_{\text{real}}$ are in gold; subplot 10(a) illustrates the synthetic variables in $\mathcal{D}_{\text{null}}$ generated using WGAN-GP Kuo et al. (2022) in brown, and subplot 10(b) depicts those in \mathcal{D}_{alt} generated with our WGAN-GP+G_EOT+VAE+Buffer in cyan.

Overall, the distributions in subplot 10(b) are more similar than those in subplot 10(a). Thus our dataset \mathcal{D}_{alt} captures more details in the ground truth $\mathcal{D}_{\text{real}}$ than Kuo et al. (2022)’s $\mathcal{D}_{\text{null}}$. Specifically, our \mathcal{D}_{alt} is more capable of representing females in gender; Asians in ethnicity; and the prescription of less common medications (e.g., NVP in the NNRTI medication class and DRV in the PI medication class). In contrast, $\mathcal{D}_{\text{null}}$ exhibits a bias towards the dominant class in the binary and categorical variables (e.g., making the medication in $\mathcal{D}_{\text{null}}$ even more unlikely to include Extra pk-En than that in $\mathcal{D}_{\text{real}}$). This hence shows that the additional VAE and extra buffer in our setup was effective in capturing extreme class imbalanced distributions in real world clinical data. Refer to Appendix A for extra results on our WGAN-GP+VAE+Buffer setup.

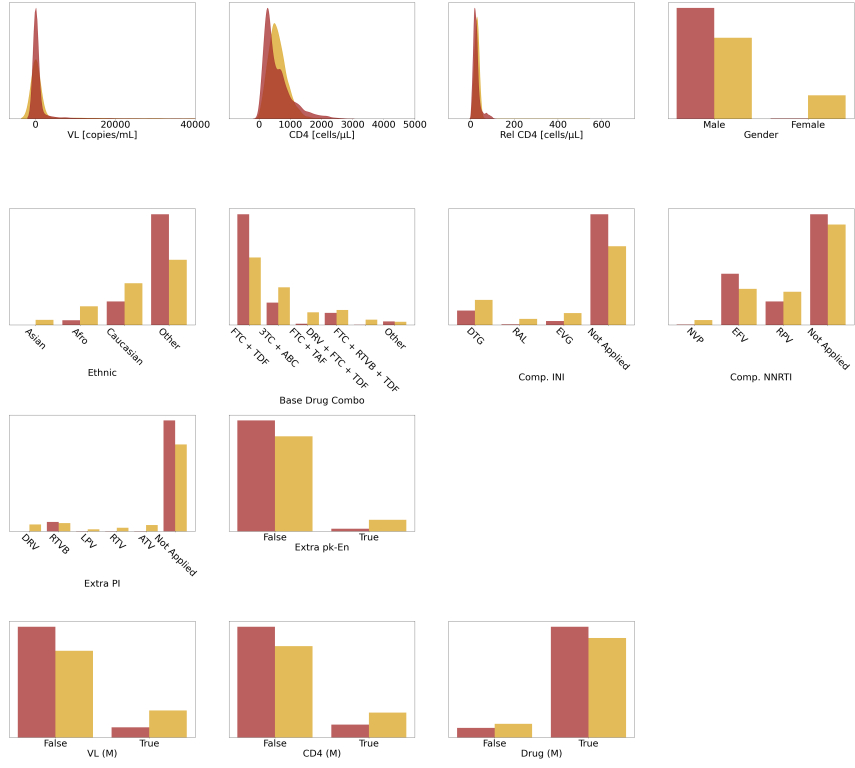
We then examined the synthetic variables using a series of hierarchically structured statistical tests outlined in Section 4.3.2. All variables of the WGAN-GP+G_EOT+VAE+Buffer synthetic dataset passed the KS test revealing that all variables of our synthetic dataset are realistic and capture both the mean and variance of their real counterparts. In contrast, the synthetic VL distribution in Kuo et al.’s WGAN-GP generated dataset failed the KS test because it was not able to mirror the spread of the real VL distribution¹¹. Refer to Appendix A for the complete statistical outcomes.

5.3 CORRELATIONS AMONG VARIABLES

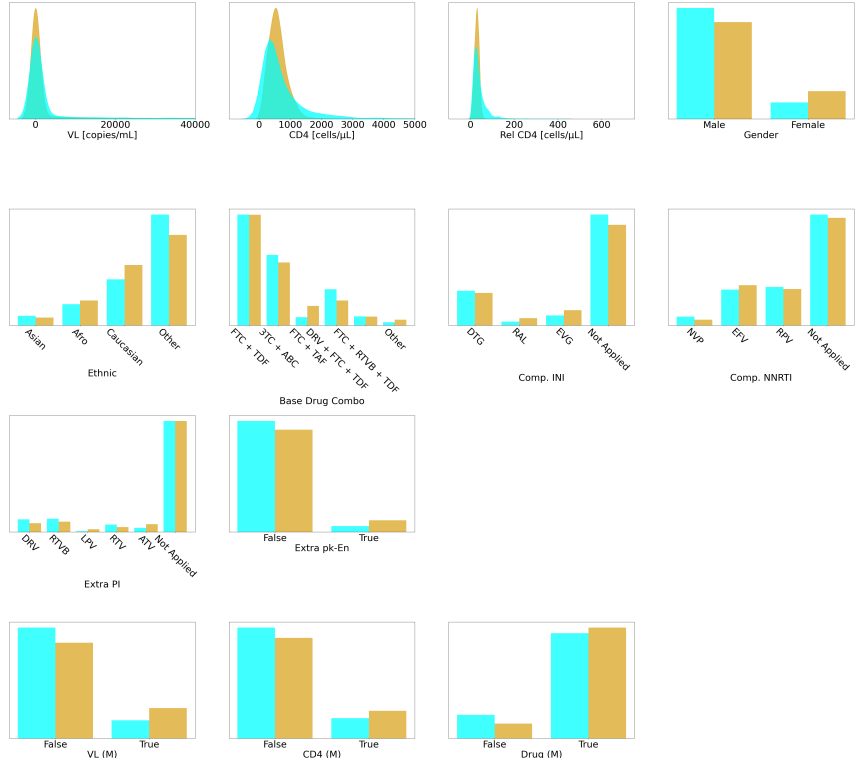
We continued to check the fidelity among variable pairs following the procedure described in Section 4.3.3. The correlations among the variables of the datasets are shown in Figure 11. Overall, Kuo et al. (2022)’s WGAN-GP and our two extended setups were all able to generate synthetic datasets with realistic correlations. This applied to both the static correlation in subplot 11(a) and the dynamic correlations in subplots 11(b) and (c).

While less significant, it can be argued that the variables in $\mathcal{D}_{\text{null}}$ generated using the baseline WGAN-GP have the tendency to increase the magnitudes of correlations. Some examples of this

¹¹See Tab. 7 on page 26 of Kuo et al. (2022).



(a) Synthetic dataset $\mathcal{D}_{\text{null}}$ from WGAN-GP (Kuo et al., 2022) in brown.



(b) Synthetic dataset \mathcal{D}_{alt} from WGAN-GP+G_EOT+VAE+Buffer (ours) in cyan.

Figure 10: Comparing the individual variable distributions, with the real dataset in colour gold.

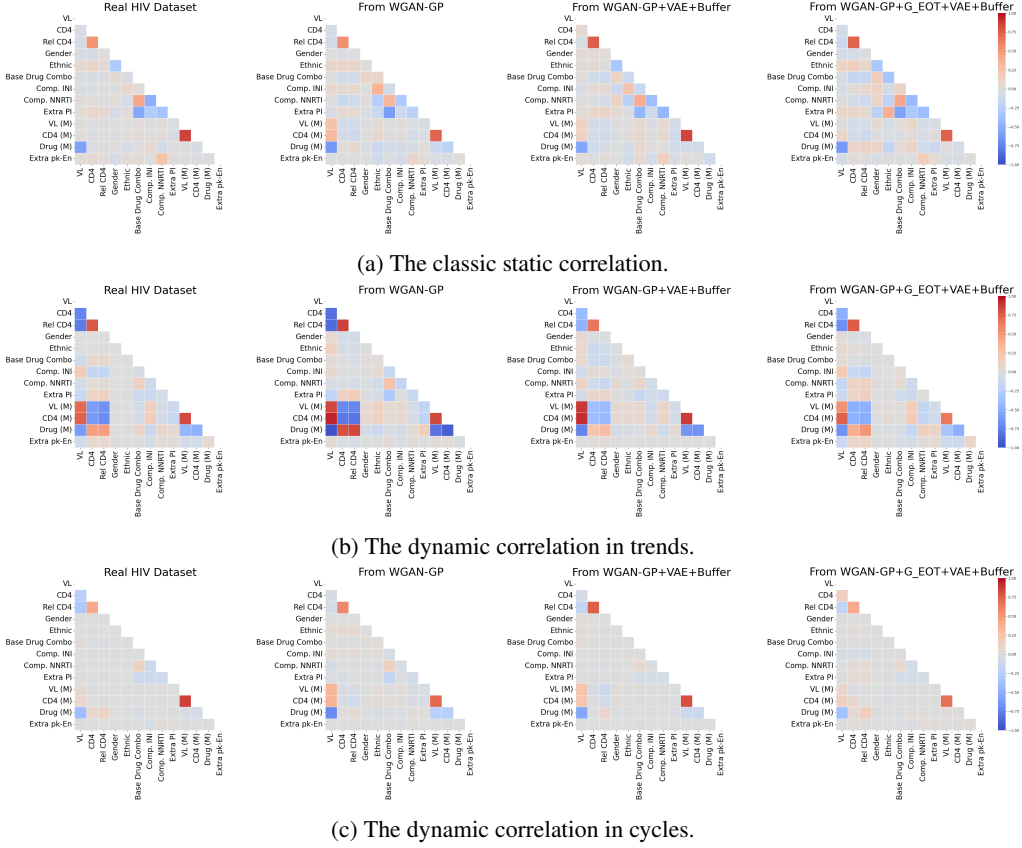


Figure 11: Comparing different types of correlations in the real and synthetic datasets.

behaviour can be found in the pairs of (Drug (M), CD4) and (Extra PI, Base Drug Combo) in the dynamic correlation in trends; and likewise for (CD4 (M), VL) in the dynamic correlations in cycles.

In contrast, it could be argued that the correlations between variables in \mathcal{D}_{alt} generated using our [WGAN-GP+G_EOT+VAE+Buffer](#) tend to be weaker than those in the real dataset. This is observed in (CD4, VL) in the dynamic correlation in trends and similarly in (CD4 (M), VL (M)) in the dynamic correlation in cycles.

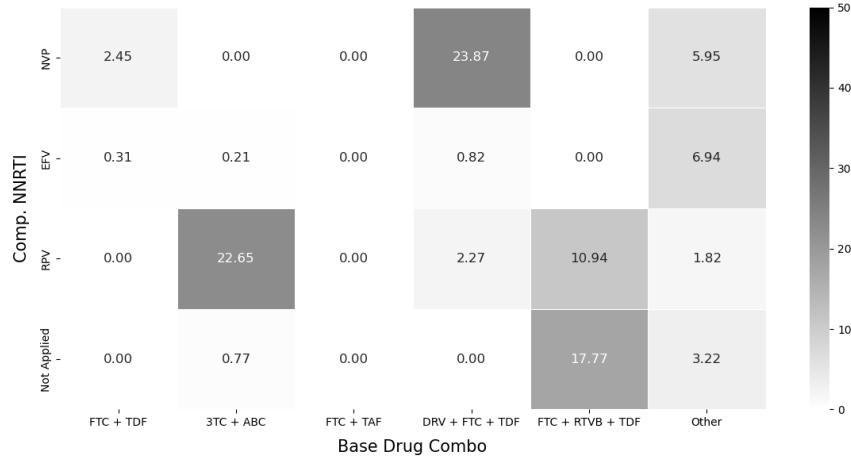
5.4 THE PATIENT DISCLOSURE RISK

Since our aim is to create realistic synthetic data available for public access, we evaluated the risk of patient re-identification as discussed in Section 4.3.4. The minimum Euclidean distance between the real dataset and the synthetic dataset generated using [WGAN-GP+VAE+Buffer](#) is 0.1029. It is 0.1229 with the synthetic dataset generated via [WGAN-GP+G_EOT+VAE+Buffer](#). Hence no real record is leaked into the synthetic dataset using either of our setups. Note, it is not meaningful to compare the magnitudes of the Euclidean distances and what we desire is that both > 0 .

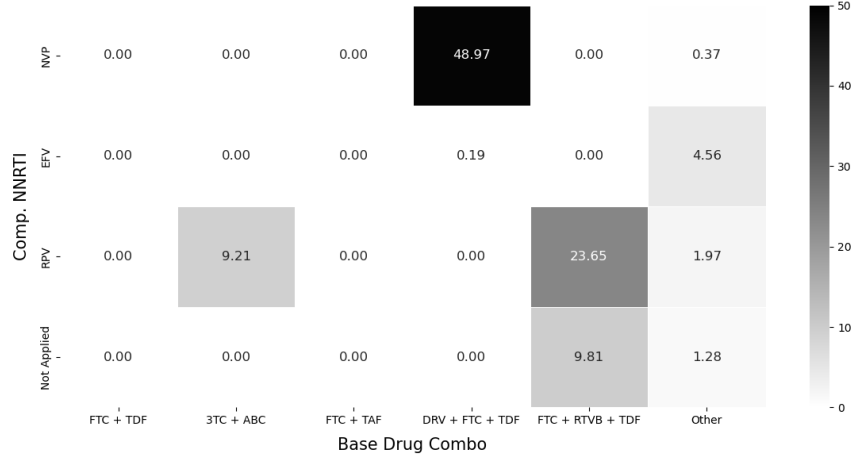
Using [El Emam et al. \(2020\)](#)'s metric, the disclosure risk of [WGAN-GP+VAE+Buffer](#)'s synthetic dataset is 0.081% while it is 0.084% for [WGAN-GP+G_EOT+VAE+Buffer](#)'s synthetic dataset. In comparison, the risk is 0.041% for [WGAN-GP](#) (see page 9 of [Kuo et al. \(2022\)](#)). All of the results are much lower than the 9% threshold suggested by the [World Health Organisation \(2016\)](#). Thus combined with our prior results in this section, we conclude that our synthetic ART for HIV datasets generated using our extended WGAN-GP setup are both realistic and secure.

5.5 DATA UTILITY

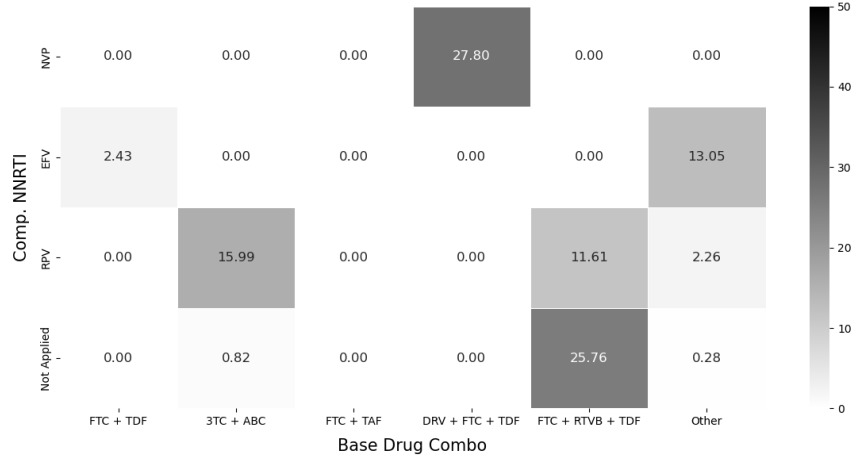
We followed the descriptions in Section 4.3.5 and tested the utility of the synthetic datasets via training RL agents to suggest clinical treatments. We visualised the relative frequencies of the



(a) Trained using the real dataset $\mathcal{D}_{\text{real}}$.

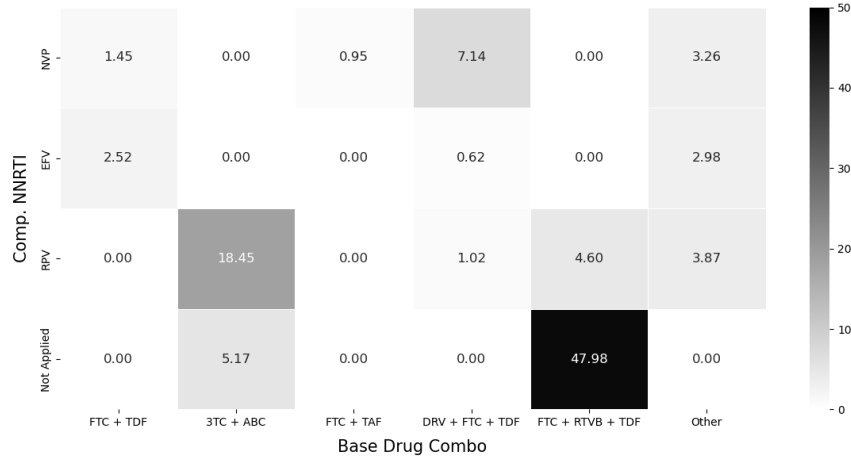


(b) Trained using the synthetic dataset $\mathcal{D}_{\text{null}}$ generated from [WGAN-GP](#) (Kuo et al., 2022).

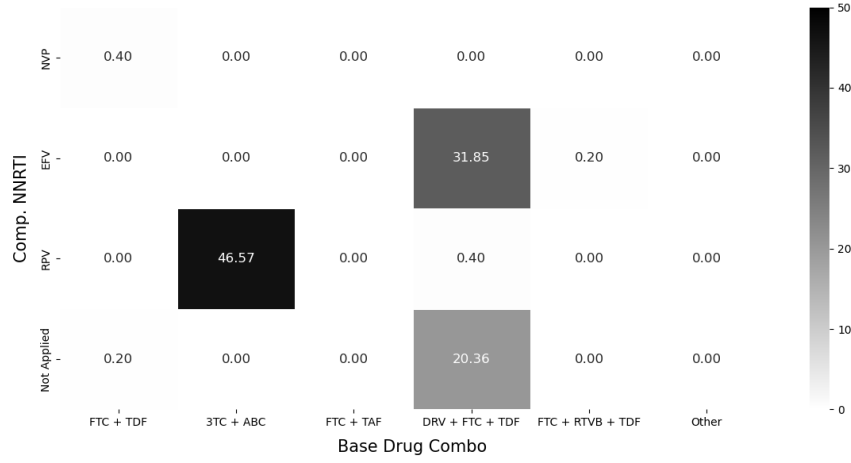


(c) Trained using the synthetic dataset \mathcal{D}_{alt} generated from our [WGAN-GP+G_EOT+VAE+Buffer](#).

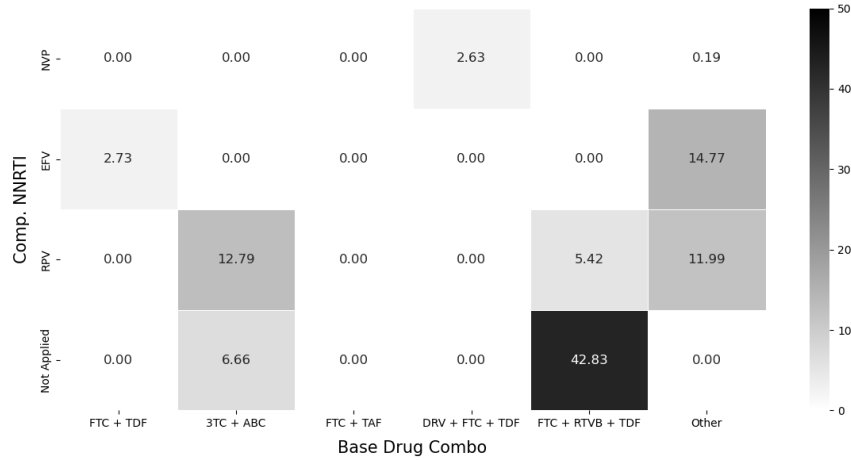
Figure 12: The suggestions made by RL agents trained on different ART for HIV datasets with Comp. NNRTI and Base Drug Combo spanning the action space.



(a) Trained using the real dataset $\mathcal{D}_{\text{real}}$.



(b) Trained using the synthetic dataset $\mathcal{D}_{\text{null}}$ generated from [WGAN-GP](#) ([Kuo et al., 2022](#)).



(c) Trained using the synthetic dataset \mathcal{D}_{alt} generated from our [WGAN-GP+G_EOT+VAE+Buffer](#).

Figure 13: The suggestions made by RL agents trained on African patients in different ART for HIV datasets with Comp. NNRTI and Base Drug Combo spanning the action space.

actions taken by the trained RL agents using heatmaps. Each tile represents a unique action, and the number on the tile represents the frequency of that action, as a proportion of all actions. This section primarily focuses on the synthetic dataset generated using [WGAN-GP+G_EOT+VAE+Buffer](#) as our default \mathcal{D}_{alt} .

5.5.1 GENERAL UTILITY

Figure 12 illustrates the actions taken by the RL agents when the action space was spanned by Comp. NNRTI and Base Drug Combo. Subplot (a) presents the actions taken by an RL agent trained using the real dataset \mathcal{D}_{real} ; subplot (b) is when the RL agent was trained on the synthetic dataset \mathcal{D}_{null} generated by [WGAN-GP](#) (Kuo et al., 2022); and likewise subplot (c) for an RL agent trained on the synthetic dataset \mathcal{D}_{alt} generated using our [WGAN-GP+G_EOT+VAE+Buffer](#).

The heatmap in subplot (b) does not match the one in subplot (a), indicating that the RL agent trained using \mathcal{D}_{null} generated from [WGAN-GP](#) was incapable of suggesting similar actions to the RL agent trained using \mathcal{D}_{real} . The RL agent trained on \mathcal{D}_{null} suggested NVP for Comp. NRTI with DRV + FTC + TDF for Base Drug Combo for 48.97% of all its actions. The undiversified policy was likely induced by mode collapse in [WGAN-GP](#) – causing \mathcal{D}_{null} to capture only a fraction of all possible treatments prescribed in real life (see Table 3 and Figure 6).

In contrast, subplot (c) shows that the RL agent trained using \mathcal{D}_{alt} generated by [WGAN-GP+G_EOT+VAE+Buffer](#) exhibited a higher diversification in its strategy to suggest treatment. The heat map in subplot (c) mirrored the one in subplot (a) better, showing that our synthetic dataset \mathcal{D}_{alt} possesses a higher utility than the baseline \mathcal{D}_{null} . See more results in Appendix B, where the action space is spanned by Comp. INI and Base Drug Combo.

5.5.2 UTILITY IN MINORITY GROUPS

Mode collapse in GANs has a particularly negative impact on the downstream model utility for minority groups. To demonstrate the severity, we repeated the experiments in Section 5.5.1 but only with patients of African ethnicity. The results for the experiments are shown in Figure 13.

As previously demonstrated in Figure 6, Kuo et al. (2022)’s [WGAN-GP](#) experienced mode collapse and had difficulties in generating synthetic patients of Asian and African ethnicity. This meant that there weren’t many data points in \mathcal{D}_{null} to cover the diversity in the ART for HIV regimens for these minority patients. As a result, subplot 13(b) differs greatly from subplot 13(a) and the RL agent trained using \mathcal{D}_{null} was incapable of suggesting similar actions to the RL agent trained using \mathcal{D}_{real} .

In stark contrast, subplot 13(c) captures most features that can be found in subplot 13(a). This shows that our synthetic dataset \mathcal{D}_{alt} has high utility and is more suitable to replace the baseline \mathcal{D}_{null} for supporting the development of downstream machine learning algorithms. As discussed in Section 5.1, this is made possible because our [WGAN-GP+G_EOT+VAE+Buffer](#) was effective in mitigating mode collapse in generating real world clinical data.

6 DISCUSSION

This paper introduced techniques to support WGAN-GP in mitigating mode collapse when synthesising realistic clinical time-series datasets. Inspired by the work of Larsen et al. (2016) (see Sections 3.2 and 3.3), we introduced an additional VAE to the conventional WGAN-GP setup to forward information about the latent structure of the real data to the GAN generator. Furthermore, in order to enhance GAN’s ability to generate realistic data, we decided to employ an extra buffer (see Section 3.2) to replay the exact combinations of latent features of real data (in an otherwise large and sparse feature representation space).

We tested seven variants of GAN setups (see Sections 4.2 and 5) – comparing both our techniques against Kuo et al. (2022)’s [WGAN-GP](#) and prior methods that mitigated mode collapse for image generation. We found that all baselines were not effective in mitigating mode collapse for clinical time series data; hence they could not capture details of all imbalanced variables (see Figure 6 and Table 3). Using ART for HIV from the EuResist database (Zazzi et al., 2012) as a case study, we found that mode collapse in the baseline GANs caused the models to neglect the creation of synthetic patients of minority demographics (Asians and Africans, see Figure 6(b)). Likewise, we also

observed that mode collapse caused the baseline GANs to not be able to learn the imbalanced distribution in medication usage (see Figure 10(a)). In stark contrast, our synthetic datasets generated using our extended GAN setup (*i.e.*, `WGAN-GP+G_EOT+VAE+Buffer`) achieved a higher level of synthetic patient cohort diversity.

We further showed that the diversity in synthetic datasets greatly impacted their utility for supporting the development of downstream model building (see Section 5.5). RL agents trained using our synthetic dataset \mathcal{D}_{alt} were able to suggest similar actions to those trained on the real dataset $\mathcal{D}_{\text{real}}$. This was not achieved using Kuo et al. (2022)’s synthetic dataset $\mathcal{D}_{\text{null}}$ as their `WGAN-GP` experienced mode collapse. The differences in the suggested actions were particularly different when treating patients of minority background (*e.g.*, African, see Figure 13); showing that synthetic datasets generated from a GAN model that experienced mode collapse could potentially cause indirect harm in patient care.

The proposed approach improves both the *resemblance* and the *representation* (Bhanot et al., 2021) of synthetic data generated by GAN-based methods. Resemblance indicates how closely the synthetic data match the real data, and representation is used in the context of fairness to indicate how adequately priority populations are represented in the generated data (Thomasian et al., 2021). These concepts are receiving increasing attention and echo the ethic guidelines in artificial intelligence published by the Australian Government Department of Industry, Science, and Resources (2019) and the United States of America Government Food and Drug Administration (2021).

The technique introduced in this paper is currently only tested on ART for HIV. In future work, we aim to test our `WGAN-GP+G_EOT+VAE+Buffer` model on additional clinical datasets. This could be particularly interesting because Kuo et al. (2022) noted that while their `WGAN-GP` had some shortcomings in generating ART for HIV data, `WGAN-GP` performed favourably on acute hypotension (Gottesman et al., 2020) and sepsis (Komorowski et al., 2018) datasets. In contrast to ART for HIV, the latter datasets mainly comprise numeric variables. The appropriate use cases of `WGAN-GP+G_EOT+VAE+Buffer` should thus be further analysed.

While we found our synthetic dataset to be realistic, safe, and to have high utility, the generated synthetic dataset should still not be regarded as a direct replacement for the real dataset. In this paper, we used batch-constrained Q-learning to evaluate whether our synthetic dataset could be used to train RL agents; and in future work, we intend to conduct a more thorough evaluation covering more complicated algorithms including recent advancements in offline RL. Also in future work, we aim to compare GAN-based models with alternative generative models including diffusion models (Dhariwal & Nichol, 2021).

7 CONCLUSION

This paper introduced an additional VAE and an extra buffer to support `WGAN-GP` in synthesising realistic clinical time-series datasets. Using ART for HIV as a case study, we demonstrated that our resulting synthetic dataset

- achieves a better level of cohort diversity;
- mirrors the distributions of all real variables;
- accurately captures the correlations among the real variables;
- has high security and protects the identity of real patients; and
- possesses high utility to support the development of downstream machine learning models.

Of note, improvements in synthetic data quality were particularly marked in data subsets related to minority groups.

Data Access and Descriptions

Our synthetic dataset generated using `WGAN-GP+G_EOT+VAE+Buffer` is hosted on our website <https://healthgym.ai/> and is publicly accessible. The synthetic ART for HIV dataset is 44.7 MB; and is stored as a *comma separated value* (CSV) file.

There are 8,916 patients in the data and records for each patient span 60 months. The data is summarised monthly; there are hence 534,960 ($=8,916 \times 60$) rows (records) in total. There are 15 columns – including the 13 ART for HIV variables as shown in Table 1, a variable indicating the patient identifier, and a variable specifying the time point.

REFERENCES

- Martin Arjovsky, Soumith Chintala, and Léon Bottou. Wasserstein generative adversarial networks. In *the International Conference on Machine Learning*, pp. 214–223, 2017.
- Dzmitry Bahdanau, Kyung Hyun Cho, and Yoshua Bengio. Neural machine translation by jointly learning to align and translate. In *the International Conference on Learning Representations*, 2015.
- Yoshua Bengio, Jérôme Louradour, Ronan Collobert, and Jason Weston. Curriculum learning. In *the International Conference on Machine Learning*, pp. 41–48, 2009.
- Diane E Bennett, Silvia Bertagnolio, Donald Sutherland, and Charles F Gilks. The world health organisation’s global strategy for prevention and assessment of hiv drug resistance. *Antiviral Therapy*, 13(2_suppl):1–13, 2008.
- Karan Bhanot, Miao Qi, John S Erickson, Isabelle Guyon, and Kristin P Bennett. The Problem of Fairness in Synthetic Healthcare Data. *Entropy*, 23(9):1165, 2021.
- Ramiro Camino, Christian Hammerschmidt, and Radu State. Generating multi-categorical samples with generative adversarial networks. In *the ICML Workshop on Theoretical Foundations and Applications of Deep Generative Models*, 2018.
- Edward Choi, Siddharth Biswal, Bradley Malin, Jon Duke, Walter F Stewart, and Jimeng Sun. Generating multi-label discrete patient records using generative adversarial networks. In *the Machine Learning for Healthcare Conference*, pp. 286–305, 2017.
- CKCN Chow and Cong Liu. Approximating discrete probability distributions with dependence trees. *IEEE Transactions on Information Theory*, 14(3):462–467, 1968.
- Richard A Davis, Keh-Shin Lii, and Dimitris N Politis. Remarks on some nonparametric estimates of a density function. In *Selected Works of Murray Rosenblatt*, pp. 95–100, 2011.
- Prafulla Dhariwal and Alexander Nichol. Diffusion models beat gans on image synthesis. In *the Advances in Neural Information Processing Systems*, pp. 8780–8794, 2021.
- David B Dunson and Chuanhua Xing. Nonparametric bayes modelling of multivariate categorical data. *Journal of the American Statistical Association*, 104(487):1042–1051, 2009.
- Khaled El Emam, Lucy Mosquera, and Jason Bass. Evaluating identity disclosure risk in fully synthetic health data: Model development and validation. *Journal of Medical Internet Research*, 22:23139, 2020.
- Stephen E Fienberg and Russell J Steele. Disclosure limitation using perturbation and related methods for categorical data. *Journal of Official Statistics*, 14:485, 1998.
- Scott Fujimoto, David Meger, and Doina Precup. Off-policy deep reinforcement learning without exploration. In *the International Conference on Machine Learning*, pp. 2052–2062, 2019.
- Andre Goncalves, Priyadip Ray, Braden Soper, Jennifer Stevens, Linda Coyle, and Ana Paula Sales. Generation and evaluation of synthetic patient data. *BMC Medical Research Methodology*, 20:1–40, 2020.
- Ian Goodfellow. Neurips 2016 tutorial: Generative adversarial networks, 2016. Preprint at <https://arxiv.org/abs/1701.00160>.
- Ian Goodfellow, Jean Pouget-Abadie, Mehdi Mirza, Bing Xu, David Warde-Farley, Sherjil Ozair, Aaron Courville, and Yoshua Bengio. Generative adversarial nets. In *the Advances in Neural Information Processing Systems*, 2014.
- Omer Gottesman, Joseph Futoma, Yao Liu, Sonali Parbhoo, Leo Celi, Emma Brunskill, and Finale Doshi-Velez. Interpretable off-policy evaluation in reinforcement learning by highlighting influential transitions. In *the International Conference on Machine Learning*, pp. 3658–3667, 2020.

-
- Alex Graves, Santiago Fernández, and Jürgen Schmidhuber. Bidirectional lstm networks for improved phoneme classification and recognition. In *the International Conference on Artificial Neural Networks*, pp. 799–804, 2005.
- Ishaan Gulrajani, Faruk Ahmed, Martin Arjovsky, Vincent Dumoulin, and Aaron C Courville. Improved training of wasserstein gans. In I. Guyon, U. V. Luxburg, S. Bengio, H. Wallach, R. Fergus, S. Vishwanathan, and R. Garnett (eds.), *the Advances in Neural Information Processing Systems*, 2017.
- Kaiming He, Xiangyu Zhang, Shaoqing Ren, and Jian Sun. Deep residual learning for image recognition. In *the IEEE Conference on Computer Vision and Pattern Recognition*, pp. 770–778, 2016.
- Sepp Hochreiter and Jürgen Schmidhuber. Long short-term memory. *Neural Computation*, 9:1735–1780, 1997.
- John L Hodges. The significance probability of the smirnov two-sample test. *Arkiv för Matematik*, 3(5):469–486, 1958.
- Tero Karras, Samuli Laine, and Timo Aila. A style-based generator architecture for generative adversarial networks. In *the IEEE Conference on Computer Vision and Pattern Recognition*, pp. 4401–4410, 2019.
- Maurice G Kendall. The treatment of ties in ranking problems. *Biometrika*, 33:239–251, 1945.
- Jacob Devlin Ming-Wei Chang Kenton and Lee Kristina Toutanova. Bert: Pre-training of deep bidirectional transformers for language understanding. In *the Conference of the North American Chapter of the Association for Computational Linguistics*, pp. 4171–4186, 2019.
- Diederik P. Kingma and Jimmy Ba. Adam: A method for stochastic optimisation. In *the International Conference on Learning Representations*, 2015.
- Diederik P Kingma and Max Welling. Auto-encoding variational bayes. In *the International Conference on Learning Representations*, 2014.
- Naveen Kodali, Jacob Abernethy, James Hays, and Zsolt Kira. On convergence and stability of gans, 2017. Preprint at <https://arxiv.org/abs/1705.07215>.
- Matthieu Komorowski, Leo A Celi, Omar Badawi, Anthony C Gordon, and A Aldo Faisal. The artificial intelligence clinician learns optimal treatment strategies for sepsis in intensive care. *Nat. Med.*, 24:1716–1720, 2018.
- Nicholas I Kuo, Mehrtash Harandi, Nicolas Fourier, Christian Walder, Gabriela Ferraro, and Hanna Suominen. Learning to continually learn rapidly from few and noisy data. In *the Meta-Learning and Co-Hosted Competition of the AAAI Conference on Artificial Intelligence*, pp. 65–76, 2021.
- Nicholas I Kuo, Mark N Polizzotto, Simon Finfer, Federico Garcia, Anders Sönnnerborg, Maurizio Zazzi, Michael Böhm, Rolf Kaiser, Louisa Jorm, Sebastiano Barbieri, et al. The health gym: Synthetic health-related datasets for the development of reinforcement learning algorithms. *Scientific Data*, 9(1):1–24, 2022.
- Anders Boesen Lindbo Larsen, Søren Kaae Sønderby, Hugo Larochelle, and Ole Winther. Autoencoding beyond pixels using a learned similarity metric. In *the International Conference on Machine Learning*, pp. 1558–1566, 2016.
- Sergey Levine, Aviral Kumar, George Tucker, and Justin Fu. Offline reinforcement learning: Tutorial, review, and perspectives on open problems, 2020. Preprint at <https://arxiv.org/abs/2005.01643>.
- Chun-Liang Li, Wei-Cheng Chang, Yu Cheng, Yiming Yang, and Barnabás Póczos. Mmd gan: Towards deeper understanding of moment matching network. In *the Advances in Neural Information Processing Systems*, pp. 2200–2210, 2017.
- Jin Li, Benjamin J Cairns, Jingsong Li, and Tingting Zhu. Generating synthetic mixed-type longitudinal electronic health records for artificial intelligent applications, 2021. Preprint at <https://arxiv.org/abs/2112.12047>.

-
- Kanglin Liu, Wenming Tang, Fei Zhou, and Guoping Qiu. Spectral regularisation for combating mode collapse in gans. In *the IEEE International Conference on Computer Vision*, pp. 6382–6390, 2019.
- Ran Liu, Joseph L Greenstein, James C Fackler, Jules Bergmann, Melania M Bembea, and Raymond L Winslow. Offline reinforcement learning with uncertainty for treatment strategies in sepsis, 2021. Preprint at <https://arxiv.org/abs/2107.04491>.
- Karttikeya Mangalam and Rohin Garg. Overcoming mode collapse with adaptive multi adversarial training, 2021. Preprint at <https://arxiv.org/abs/2112.14406>.
- Michael McCloskey and Neal J Cohen. Catastrophic interference in connectionist networks: The sequential learning problem. In *Psychology of Learning and Motivation*, volume 24, pp. 109–165, 1989.
- Lars Mescheder, Andreas Geiger, and Sebastian Nowozin. Which training methods for gans do actually converge? In *the International Conference on Machine Learning*, pp. 3481–3490, 2018.
- Luke Metz, Ben Poole, David Pfau, and Jascha Sohl-Dickstein. Unrolled generative adversarial networks. In *the International Conference on Learning Representations*, 2016.
- Tomas Mikolov, Ilya Sutskever, Kai Chen, Greg S Corrado, and Jeff Dean. Distributed representations of words and phrases and their compositionality. In *the Advances in Neural Information Processing Systems*, pp. 3111–3119, 2013.
- Gonalo Mordido, Haojin Yang, and Christoph Meinel. microbatchgan: Stimulating diversity with multi-adversarial discrimination. In *the IEEE Winter Conference on Applications of Computer Vision*, pp. 3061–3070, 2020.
- Alejandro Mottini, Alix Lheritier, and Rodrigo Acuna-Agost. Airline passenger name record generation using generative adversarial networks, 2018. Preprint at <https://arxiv.org/abs/1807.06657>.
- Mavuto M Mukaka. A guide to appropriate use of correlation coefficient in medical research. *Malawi Medical Journal*, 24:69–71, 2012.
- Sonali Parbhoo, Jasmina Bogojenska, Maurizio Zazzi, Volker Roth, and Finale Doshi-Velez. Combining kernel and model based learning for hiv therapy selection. *AMIA Summits on Translational Science Proceedings*, 2017:239, 2017.
- Santiago Pascual, Antonio Bonafonte, and Joan Serra. Segan: Speech enhancement generative adversarial network. *Interspeech*, pp. 3642–3646, 2017.
- Mattia CF Prosperi, Michal Rosen-Zvi, Andr  Altman, Maurizio Zazzi, Simona Di Giambenedetto, Rolf Kaiser, Eugen Sch lter, Daniel Struck, Peter Sloot, David A Van De Vijver, et al. Antiretroviral therapy optimisation without genotype resistance testing: a perspective on treatment history based models. *PloS one*, 5:e13753, 2010.
- Friedrich Pukelsheim. The three sigma rule. *The American Statistician*, 48:88–91, 1994.
- Alec Radford, Luke Metz, and Soumith Chintala. Unsupervised representation learning with deep convolutional generative adversarial networks, 2015. Preprint at <https://arxiv.org/abs/1511.06434>.
- Alec Radford, Karthik Narasimhan, Tim Salimans, and Ilya Sutskever. Improving language understanding by generative pre-training. In *a Technical Report of OpenAI*, 2018.
- Sylvestre-Alvise Rebuffi, Alexander Kolesnikov, Georg Sperl, and Christoph H Lampert. icarl: Incremental classifier and representation learning. In *the IEEE Conference on Computer Vision and Pattern Recognition*, pp. 2001–2010, 2017.
- David E Rumelhart, Geoffrey E Hinton, and Ronald J Williams. Learning representations by back-propagating errors. *Nature*, 323:533–536, 1986.

-
- Tim Salimans, Ian Goodfellow, Wojciech Zaremba, Vicki Cheung, Alec Radford, and Xi Chen. Improved techniques for training gans. In *the Advances in Neural Information Processing Systems*, pp. 2234–2242, 2016.
- George W Snedecor and Witiiam G Cochran. Statistical methods. Ames: Iowa State Univ. Press Iowa, 54:71–82, 1989.
- Jascha Sohl-Dickstein, Eric Weiss, Niru Maheswaranathan, and Surya Ganguli. Deep unsupervised learning using nonequilibrium thermodynamics. In *the International Conference on Machine Learning*, pp. 2256–2265, 2015.
- Casper Kaae Sønderby, Jose Caballero, Lucas Theis, Wenzhe Shi, and Ferenc Huszár. Amortised map inference for image super-resolution. In *the International Conference on Learning Representations*, 2016.
- Akash Srivastava, Lazar Valkov, Chris Russell, Michael U Gutmann, and Charles Sutton. Veegan: Reducing mode collapse in gans using implicit variational learning. In *the Advances in Neural Information Processing Systems*, pp. 3310–3320, 2017.
- Richard S Sutton and Andrew G Barto. *Reinforcement Learning: An Introduction*. MIT Press, 2018.
- Michele W Tang, Tommy F Liu, and Robert W Shafer. The HIVdb System for HIV-1 Genotypic Resistance Interpretation. *Intervirology*, 55(2):98–101, 2012.
- Australian Government Department of Industry, Science, and Resources. Australia’s artificial intelligence ethics framework, 2019. Access through <https://www.industry.gov.au/publications/australias-artificial-intelligence-ethics-framework>.
- European Medicines Agency. European medicines agency policy on publication of clinical data for medical products for human use, 2014. Access through http://www.ema.europa.eu/docs/en_GB/document_library/Other/2014/10/WC500174796.pdf.
- Health Canada. Guidance document on public release of clinical information, 2014. Access through <https://www.canada.ca/en/health-canada/services/drug-health-product-review-approval/profile-public-release-clinical-information-guidance/document.html>.
- United States of America Government Food and Drug Administration. Artificial intelligence/machine learning (ai/ml)-based software as a medical device (samd) action plan, 2021. Access through <https://www.fda.gov/media/145022/download>.
- Hoang Thanh-Tung and Truyen Tran. Catastrophic forgetting and mode collapse in gans. In *the International Joint Conference on Neural Networks*, pp. 1–10, 2020.
- Nicole M Thomasian, Carsten Eickhoff, and Eli Y Adashi. Advancing health equity with artificial intelligence. *Journal of Public Health Policy*, pp. 1–10, 2021.
- Laurens Van der Maaten and Geoffrey Hinton. Visualising data using t-sne. *Journal of Machine Learning Research*, 9(11), 2008.
- Aaron Van Oord, Nal Kalchbrenner, and Koray Kavukcuoglu. Pixel recurrent neural networks. In *the International Conference on Machine Learning*, pp. 1747–1756, 2016.
- Sergei Vassilvitskii and David Arthur. k-means++: The advantages of careful seeding. In *Proceedings of the ACM-SIAM Symposium on Discrete Algorithms*, pp. 1027–1035, 2006.
- Ashish Vaswani, Noam Shazeer, Niki Parmar, Jakob Uszkoreit, Llion Jones, Aidan N Gomez, Łukasz Kaiser, and Illia Polosukhin. Attention is all you need. *the Advances in Neural Information Processing Systems*, pp. 6000–6010, 2017.

-
- Jason Walonoski, Mark Kramer, Joseph Nichols, Andre Quina, Chris Moesel, Dylan Hall, Carlton Duffett, Kudakwashe Dube, Thomas Gallagher, and Scott McLachlan. Synthea: An approach, method, and software mechanism for generating synthetic patients and the synthetic electronic health care record. *Journal of the American Medical Informatics Association*, 25:230–238, 2018.
- Jacob A. Wegelin. A survey of partial least squares (pls) methods, with emphasis on the two-block case. Technical report, University of Washington, 2000.
- Max Welling. Herding dynamical weights to learn. In *the International Conference on Machine Learning*, pp. 1121–1128, 2009.
- Mi-Ja Woo, Jerome P Reiter, Anna Oganian, and Alan F Karr. Global measures of data utility for microdata masked for disclosure limitation. *Journal of Privacy and Confidentiality*, 1, 2009.
- World Health Organisation. Consolidated guidelines on the use of antiretroviral drugs for treating and preventing hiv infection: Recommendations for a public health approach, 2016. Access through <https://www.who.int/publications/i/item/9789241549684>.
- Jingjing Xu, Xuancheng Ren, Junyang Lin, and Xu Sun. Diversity-promoting gan: A cross-entropy based generative adversarial network for diversified text generation. In *the Empirical Methods in Natural Language Processing*, pp. 3940–3949, 2018.
- Jiahui Yu, Zhe Lin, Jimei Yang, Xiaohui Shen, Xin Lu, and Thomas S Huang. Generative image inpainting with contextual attention. In *the IEEE Conference on Computer Vision and Pattern Recognition*, pp. 5505–5514, 2018.
- Karen K Yuen. The two-sample trimmed t for unequal population variances. *Biometrika*, 61:165–170, 1974.
- Maurizio Zazzi, Francesca Incardona, Michal Rosen-Zvi, Mattia Prosperi, Thomas Lengauer, Andre Altmann, Anders Sonnerborg, Tamar Lavee, Eugen Schülter, and Rolf Kaiser. Predicting response to antiretroviral treatment by machine learning: the euresist project. *Intervirology*, 55(2):123–127, 2012.

AUTHOR CONTRIBUTIONS STATEMENT

N.K. and **S.B.** designed, implemented and validated the deep learning models used to generate the synthetic datasets. **L.J.** contributed to the design of the study and provided expertise regarding the risk of sensitive information disclosure. **M.P.** provided clinical expertise on antiretroviral therapy for HIV. **F.G.**, **A.S.**, **M.Z.**, **M.B.**, and **R.K.** contributed patient data as part of the EuResist Integrated Database. Furthermore, **N.K.** wrote the manuscript and **S.B.** and **N.K.** designed the study. All authors contributed to the interpretation of findings and manuscript revisions.

COMPETING INTERESTS

The authors declare no competing interests.

ACKNOWLEDGEMENTS

This study benefited from data provided by EuResist Network EIDB; and this project has been funded by a Wellcome Trust Open Research Fund (reference number 219691/Z/19/Z).

SUPPLEMENTARY MATERIALS

**Nicholas I-Hsien Kuo¹,
Federico Garcia², Anders Sönnnerborg³, Maurizio Zazzi⁴, Michael Böhm⁵, Rolf Kaiser⁵,
Mark Polizzotto⁶, Louisa Jorm¹, Sebastiano Barbieri¹**

¹Centre for Big Data Research in Health (CBDRH), the University of New South Wales,
Sydney, Australia

²Hospital Universitario San Cecilio, Granada, Spain

³Hospital Karolinska Institutet, Stockholm, Sweden

⁴Università degli Studi di Siena, Siena, Italy

⁵Uniklinik Köln, Universität zu Köln, Cologne, Germany

⁶Australian National University, Canberra, Australia

Corresponding author: Nicholas I-Hsien Kuo (n.kuo@unsw.edu.au)

In this study, we presented an extended setup to GAN models (Goodfellow et al., 2014) for synthesising clinical time series data. We based our work on Kuo et al. (2022)’s WGAN-GP and demonstrated the effectiveness in mitigating mode collapse (Goodfellow, 2016) on the antiretroviral therapy for human immunodeficiency virus (ART for HIV) (Zazzi et al., 2012). We conducted several experiments with different setups; and the supplementary materials include some additional interesting secondary results.

A ON THE REALISTICNESS OF INDIVIDUAL VARIABLES

Extra Results on WGAN-GP+VAE+Buffer

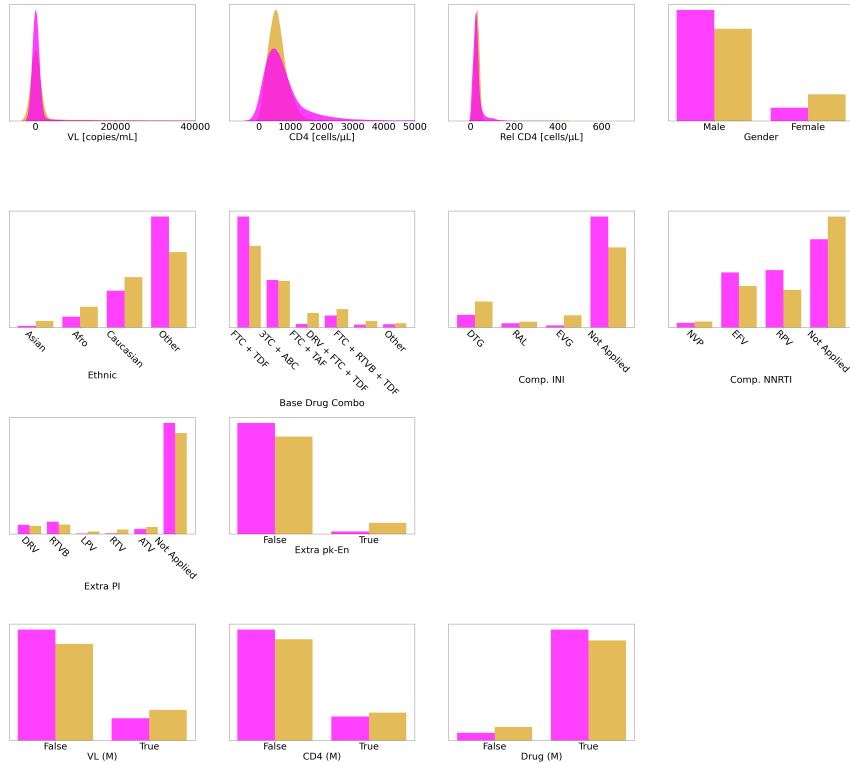


Figure 14: Comparing the individual variables of the real dataset (in colour gold) with those in the synthetic dataset generated with WGAN-GP+VAE+Buffer (in magenta).

Following Section 5.2, we plotted the variable distributions of the synthetic dataset generated using our `WGAN-GP+VAE+Buffer` in Figure 14. Compared to the baseline `WGAN-GP` (Kuo et al., 2022) in Figure 10(a), we observed that `WGAN-GP+VAE+Buffer` was more capable of capturing severe class imbalance. However, the results were less good than our `WGAN-GP+G_EOT+VAE+Buffer` setup shown in Figure 10(b); this model experienced some notable difficulties in representing categorical variables with many levels such as Extra PI and Comp. INI.

The Complete Statistical Outcome

We followed Kuo et al. (2022)’s work and computed a series of hierarchical statistical tests (see Figure 5) to verify the realisticness of the synthetic variables. The results are organised in Tables 4, 5, and 6. The purpose of the statistical tests was to check whether an arbitrary neural network would consider the synthetic dataset highly similar to the real dataset during iterative batch training. Hence for a maximum of 100 iterations (corresponding to 100 in the denominator in the tables), we sampled a batch of synthetic and real data each of batch size 32, and performed at most 4 tests along the variable dimension. Refer to App. D.5 on page 44 of Kuo et al. (2022) for the full algorithmic description.

The biggest problem in Kuo et al. (2022)’s synthetic dataset was VL which had a misaligned variance. This concern is now addressed in our datasets. While all variables in the synthetic dataset generated by our `WGAN-GP+VAE+Buffer` are realistic, we observed that there are still some misalignments in variances. Notably, the synthetic Ethnicity variable passed less than 70% of F-test (Table 5), hinting that there was a slight mode collapse problem which may have caused mismatches among the categories for this variable. In contrast, no major problem was observed in Table 6; hence all variables generated using our better performing model of `WGAN-GP+G_EOT+VAE+Buffer` are realistic.

B EXTRA RESULTS ON DATA UTILITY

Following Section 5.5.1, we continued to train RL agents using different synthetic datasets and spanned the action space through the variables Comp. INI and Base Drug Combo. The results are shown in Figure 15.

Again, we see that our synthetic dataset \mathcal{D}_{alt} possesses a higher utility than the baseline $\mathcal{D}_{\text{null}}$. The RL agent trained using $\mathcal{D}_{\text{null}}$ was incapable of suggesting similar treatments to the RL agent trained using $\mathcal{D}_{\text{real}}$. Notably, the former would suggest up to 78.13% of all its actions on EVG for Comp. INI and FTC + RTVB + TDF for Base Drug Combo. In contrast, the RL agent trained using our \mathcal{D}_{alt} suggested a more diverse treatment strategy and mirrored the behaviour of the RL agent trained using the ground truth.

Variable Name	KS-Test	t-Test	F-Test	Three Sigma Rule Test
VL	48/100	90/100	15/100	100/100
CD4	83/100	97/100	91/100	91/100
Rel CD4	85/100	92/100	100/100	99/100
Gender	97/100	--	49/100	--
Ethnic	81/100	--	38/100	--
Base Drug Combo	73/100	--	71/100	--
Comp. INI	96/100	--	73/100	--
Comp. NNRTI	92/100	--	95/100	--
Extra PI	100/100	--	73/100	--
Extra pk-En	100/100	--	95/100	--
VL (M)	100/100	--	72/100	--
CD4 (M)	99/100	--	94/100	--
Drug (M)	100/100	--	88/100	--

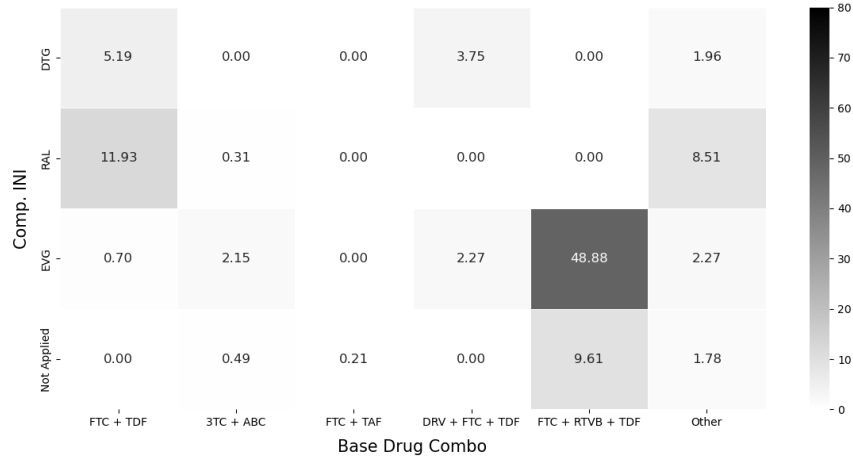
Table 4: The reference statistics taken from Tab. 11 on page 47 of [Kuo et al. \(2022\)](#)'s [WGAN-GP](#).

Variable Name	KS-Test	t-Test	F-Test	Three Sigma Rule Test
VL	73/100	95/100	39/100	100/100
CD4	87/100	92/100	91/100	91/100
Rel CD4	90/100	96/100	99/100	97/100
Gender	100/100	--	74/100	--
Ethnic	89/100	--	61/100	--
Base Drug Combo	95/100	--	82/100	--
Comp. INI	97/100	--	85/100	--
Comp. NNRTI	98/100	--	96/100	--
Extra PI	100/100	--	96/100	--
Extra pk-En	100/100	--	68/100	--
VL (M)	99/100	--	91/100	--
CD4 (M)	100/100	--	96/100	--
Drug (M)	100/100	--	88/100	--

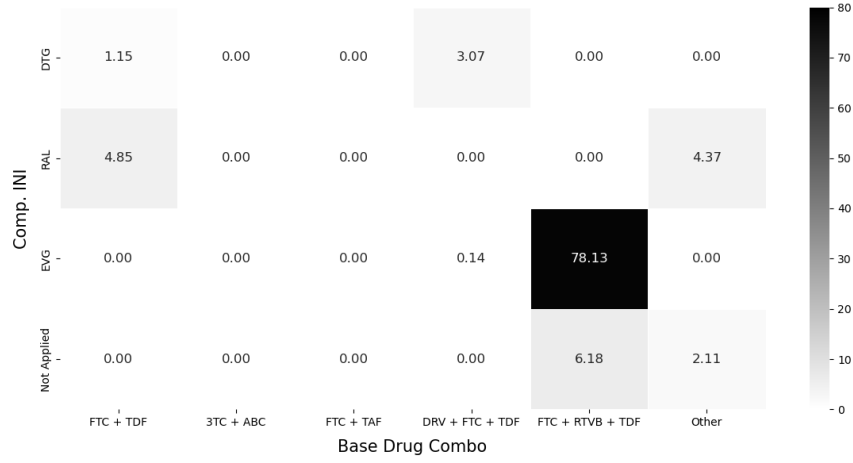
Table 5: The statistical outcomes of our [WGAN-GP+VAE+Buffer](#) synthetic dataset.

Variable Name	KS-Test	t-Test	F-Test	Three Sigma Rule Test
VL	78/100	93/100	77/100	98/100
CD4	82/100	96/100	96/100	82/100
Rel CD4	81/100	72/100	100/100	91/100
Gender	100/100	--	87/100	--
Ethnic	90/100	--	84/100	--
Base Drug Combo	95/100	--	82/100	--
Comp. INI	99/100	--	92/100	--
Comp. NNRTI	99/100	--	95/100	--
Extra PI	100/100	--	95/100	--
Extra pk-En	100/100	--	91/100	--
VL (M)	98/100	--	71/100	--
CD4 (M)	100/100	--	94/100	--
Drug (M)	100/100	--	82/100	--

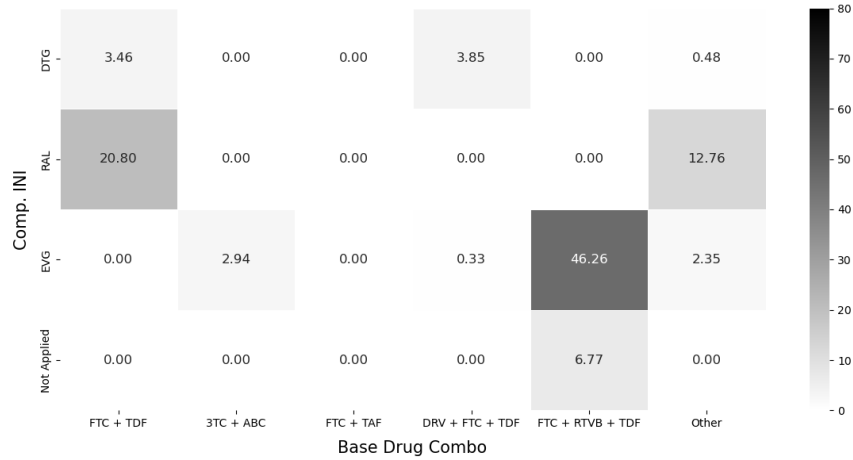
Table 6: The statistical outcomes of our [WGAN-GP+G.EOT+VAE+Buffer](#) synthetic dataset.



(a) Trained using the real dataset $\mathcal{D}_{\text{real}}$.



(b) Trained using the synthetic dataset $\mathcal{D}_{\text{null}}$ generated from [WGAN-GP](#) ([Kuo et al., 2022](#)).



(c) Trained using the synthetic dataset \mathcal{D}_{alt} generated from our [WGAN-GP+G_EOT+VAE+Buffer](#).

Figure 15: The suggestions made by RL agents trained on different ART for HIV datasets with Comp. INI and Base Drug Combo spanning the action space.